The PDIM paradox of *Mycobacterium tuberculosis*: new solutions to a persistent problem

Authors

Claire V. Mulholland, Thomas J. Wiggins†, Jinhua Cui†, Catherine Vilchèze, Saranathan Rajagopalan, Michael W. Shultis, Esmeralda Z. Reyes-Fernández, William R. Jacobs Jr., Michael Berney*

Affiliations:

Department of Microbiology and Immunology, Albert Einstein College of Medicine, Bronx, New York, USA.

*Corresponding author. Email: michael.berney@einsteinmed.edu

†These authors contributed equally to this work

Abstract

Phthiocerol dimycocerosate (PDIM) is an essential virulence lipid of *Mycobacterium tuberculosis*. *In vitro* culturing rapidly selects for spontaneous mutations that cause PDIM loss leading to virulence attenuation and increased cell wall permeability. We discovered that PDIM loss is due to a metabolic deficiency of methylmalonyl-CoA that impedes the growth of PDIM-producing bacilli. This can be remedied by supplementation with odd-chain fatty acids, cholesterol, or vitamin B_{12}. We developed a much-needed facile and scalable routine assay for PDIM production and show that propionate supplementation enhances the growth of PDIM-producing bacilli and selects against PDIM-negative mutants, analogous to *in vivo* conditions. Our results solve a major issue in tuberculosis research and exemplify how discrepancies between the host and *in vitro* nutrient environments can attenuate bacterial pathogenicity.

Main Text

The cell wall of *Mycobacterium tuberculosis* (*Mtb*) is exceptionally complex and is essential to its success as a pathogen. Phthiocerol dimycocerosates (PDIMs) are long-chain non-polar lipids found in the outermost layer of the cell wall of *Mtb* and other pathogenic slow-growing mycobacteria[1]. PDIMs play a crucial role in *Mtb* pathogenesis (reviewed in[2]), however, *Mtb* is prone to losing the ability to produce PDIM *in vitro* due to spontaneous mutation of PDIM biosynthesis genes[3,4]. Loss of PDIM biosynthesis confers a growth advantage in current mycobacterial culture media[3,5], resulting in PDIM-deficient mutants dominating cultures with successive passage[3]. As PDIM deficiency decreases virulence[5-11] and increases cell wall

permeability[12,13], spontaneous PDIM loss adversely affects experimental reliability, reproducibility, and the interpretation of results. PDIM deficiency has also been shown to reduce the vaccine efficacy of *Mycobacterium bovis* BCG Pasteur[14]. "The PDIM problem" thus presents a major challenge in tuberculosis research and has hindered progress in the field for decades. We sought to understand the underlying cause of PDIM loss and develop routine methods to enable reproducible PDIM bias-free investigations in all branches of *Mtb* research.

A tractable and scalable PDIM screen

The genetically unstable nature of the PDIM biosynthetic pathway makes routine PDIM screening essential for all branches of tuberculosis research. However, current PDIM screening approaches such as whole genome sequencing (WGS), mass spectrometry, and thin layer chromatography (TLC), are expensive, cumbersome, and require specialized equipment and expertise, further compounding the PDIM problem.

We hypothesized that the differential permeability of PDIM-positive [PDIM(+)] and PDIM-negative [PDIM(-)] *Mtb*[12,13] could be exploited to develop a simpler functional PDIM assay. To test this, we first assembled a PDIM reference strain set comprised of six BSL2-approved attenuated *Mtb* H37Rv strains with varying PDIM content (Fig. 1a, Supplementary Table 1). These strains demonstrate the heterogeneity of PDIM production commonly found in laboratory *Mtb* strains. Vancomycin – a large antimicrobial glycopeptide not normally used for *Mtb* treatment due to poor penetration, has previously been reported to be more effective against PDIM deletion mutants of *Mtb* and *M. bovis* BCG than the corresponding PDIM(+) wildtype strains[15]. Accordingly, we found that PDIM levels measured by TLC significantly correlated with vancomycin MIC_{90} and MIC_{50} in our reference strain set after 10–14 days of incubation (Supplementary Fig. 1). PDIM(+) *Mtb* $mc^{2}7902$ was also more resistant to other high molecular

weight compounds than PDIM(-) mc^{2}8398, though vancomycin gave the best differentiation (Extended Data Fig. 1a,g). Furthermore, much greater Ethidium Bromide uptake[16] was observed in mc^{2}8398 than mc^{2}7902 (Extended Data Fig. 1h), consistent with enhanced permeability of PDIM(-) strains.

Whilst an intact biosynthetic pathway is essential for PDIM production, PDIM size and abundance are dependent on the availability of the three-carbon precursor methylmalonyl-CoA (MMCoA)[17]. MMCoA is generated from propionyl-CoA by propionyl-CoA carboxylase, or, from succinyl-CoA by vitamin B_{12}-dependent MMCoA mutase (Fig. 1b). In the host, *Mtb* has access to propionyl-CoA-generating carbon sources such as cholesterol[18,19] and possibly also scavenges vitamin B_{12}[20-22]. Standard Middlebrook 7H9/OADC/glycerol media, however, lacks both a propionyl-CoA-generating carbon source and vitamin B_{12}. Propionate supplementation or growth on cholesterol as a sole carbon source have been shown to increase PDIM biosynthesis[17,23]. Accordingly, we found that the addition of 0.1 or 1.0 mM propionate preferentially increased vancomycin resistance of PDIM(+) strains in 7H9/OADC/glycerol/tyloxapol + PALM media (pantothenate, arginine, leucine, and methionine; for BSL2 auxotrophic strains), enhancing the differentiation between PDIM(+) and PDIM(-) *Mtb* while improving assay robustness and reducing time to result (Fig. 1c, and Extended Data Fig. 2). To further simplify our approach and enable scalability, we established a single concentration assay we term the 'VAN10-P assay' (Fig. 1e, Extended Data Fig. 2c and Supplementary Fig. 2). The VAN10-P assay compares growth in 10 μg/ml vancomycin with 0.1 mM propionate to no-drug controls and highly correlates with PDIM production (Fig. 1f). We additionally validated our approach using isogenic PDIM(-) (Δ*ppsD*) and complemented (Δ*ppsD*::comp) strains constructed from a PDIM(+) clone (H37Rv-SC, wildtype) (Supplementary Table 2). PDIM(+) and PDIM(-) H37Rv showed a greater

than 30-fold difference in vancomycin MIC_{90} with 0.1 mM propionate ('VAN-P' MIC) (Fig. 1g) and this was also reflected in the VAN10-P assay (Fig. 1h). Highly similar results were also obtained for *Mtb* CDC1551 and its isogenic PDIM(-) (Δ*mas*) mutant (Supplementary Fig. 3).

To confirm that increased vancomycin resistance with propionate was due to enhanced PDIM production rather than other effects such as accumulation of propionyl-CoA or methylcitrate cycle intermediates[24,25], we supplemented with vitamin B_{12} to provide an alternate route for MMCoA production via the vitamin B_{12}-dependent methylmalonyl pathway[22] (Fig. 1b). Vitamin B_{12} selectively increased the vancomycin resistance of PDIM(+) *Mtb* mirroring the effect of propionate (Fig. 1g and Extended Data Fig. 2b,c), consistent with enhanced resistance due to increased PDIM production. Leucine, a potential source of propionyl-CoA[26], did not have a marked effect on vancomycin resistance of H37Rv at the concentration provided in PALM-supplemented media (0.38 mM) (Supplementary Fig. 4a).

As Tween 80 is another detergent commonly used in *Mtb* culture media, we tested whether tyloxapol could be replaced with Tween 80 in our assay. Tween 80 is known to remove several layers of the mycobacterial cell wall including PDIM[27]. Consistent with this, Tween 80 abolished PDIM-related differences in vancomycin resistance and further increased the vancomycin sensitivity of PDIM(-) *Mtb* (Fig. 1h and Extended Data Fig. 3).

Breadth and depth of PDIM bias in tuberculosis research

Next, we determined the predictive power of our approach in a range of virulent *Mtb* strains including Erdman, HN878, KZN 4207, and two different CDC1551 and H37Rv stocks (Supplementary Table 2). VAN-P screening reliably predicted PDIM levels as determined by TLC for all these strains (Fig. 2a and Extended Data Fig. 4a–d). Furthermore, VAN-P assays outperformed WGS at diagnosing PDIM deficiencies in heterogeneous populations. TLC and

VAN10-P assays showed low PDIM levels in H37Rv-A and CDC1551-A (Fig. 2a), however, standard WGS variant calling failed to identify any PDIM mutations in these stocks, whilst an unfixed mutation was identified in Erdman (Extended Data Table 1). Low-frequency variant analysis subsequently identified putative PDIM mutations at ~10–13% frequency in each of these stocks (Extended Data Table 2), indicating they comprise a mixture of different PDIM(-) mutants. Thus, WGS is a poor predictor of PDIM levels in mixed populations as these can comprise an array of different low-frequency PDIM mutations, which can be difficult to detect by WGS.

To investigate how genetic engineering of *Mtb* strains is affected by PDIM loss we generated knockout mutants of the non-PDIM-related gene *tgs1* from a mouse-passaged H37Rv stock (H37Rv-B) using specialized transduction[28]. Surprisingly, despite this being a mouse-passaged stock, only one of eight Δ*tgs1* mutants obtained (Δ*tgs1*-7) was found to be fully PDIM(+) by VAN-P MICs (Fig. 2b). This was further validated by TLC and sequence analysis (Fig. 2c–d). Historically animal passaging was the only procedure known to select for PDIM(+) *Mtb*. However, our specialized transduction results and VAN-P assays suggested that despite animal passage this may still be a mixed population (Fig. 2a–d). Indeed, VAN10-P single colony screening confirmed that while animal passage enriched for PDIM(+) clones, PDIM-deficient strains were not completely removed (Fig. 2f, Extended Data Table 1). Consequently, using VAN10-P single colony screening, we were able to isolate single PDIM(+) clones from H37Rv-B as well as other virulent strains and from avirulent mc^{2}6230 (Extended Data Fig. 4 and Extended Data Table 1).

Strikingly, six different mutations in five different PDIM genes were identified across the seven PDIM(-) Δ*tgs1* mutants (Fig. 2d,e), emphasizing the genetic heterogeneity in the PDIM gene cluster in mixed populations. We also found two unique frameshift mutations in a 7-cytosine homopolymeric tract in *ppsC* (Extended Data Fig. 5). This region appears to be a ‘hotspot’ for

mutation as we also found *ppsC* homopolymeric tract mutations in mc^{2}6230 (Extended Data Fig. 5e) and in the literature[29,30]. Homopolymeric tracts are prone to mutations caused by slipped-strand mispairing[31] and as *Mtb* lacks a DNA mismatch repair system[32] this may lead to hypervariability in these regions, further augmenting the propensity for PDIM loss *in vitro*.

Collectively these data validate VAN-P assays as a reliable and effective method to assess PDIM levels and heterogeneity in *Mtb* populations and aid in the isolation of PDIM(+) clones. However, the data presented also strongly emphasized the need to resolve the underlying issue of PDIM loss.

MMCoA deficiency impairs the growth of PDIM(+) *Mtb*

As PDIM production is tightly coupled to *Mtb* metabolism[17], we reasoned that there may be a metabolic solution to the PDIM problem. Propionyl-CoA, an upstream precursor of PDIM, can be inhibitory to bacterial growth[33]. The major pathways for propionyl-CoA detoxification are the methylcitrate cycle[34], the methylmalonyl pathway[22], and the incorporation into PDIM and other virulence-associated lipids[35,36] (Fig. 1b). We hypothesized that PDIM-deficient strains would be more sensitive to propionate toxicity without this sink for propionyl-CoA metabolism and that this could be exploited to create a PDIM selective medium. Consistent with this hypothesis, the PDIM(-) strains in our reference strain set were more sensitive to propionate than the PDIM(+) (Fig. 3a). Surprisingly, we also observed that PDIM(+) strains reached higher density at lower propionate concentrations (Fig. 3a), suggesting sub-toxic propionate may provide a growth advantage to PDIM(+) *Mtb*.

Next, we compared the growth of isogenic PDIM(+) and PDIM(-) *Mtb* with propionate and other supplements. Notably, we found that the addition of 0.1 or 1.0 mM propionate to standard 7H9/OADC/glycerol/tyloxapol media increased the growth rate of PDIM(+) strains to that of

PDIM(-) (Fig. 3c and Extended Data Fig. 6b,c). Vitamin B_{12} also restored PDIM(+) growth analogous to propionate (Fig. 3d). Again, we did not observe comparable effects when tyloxapol was replaced with Tween 80 (Extended Data Fig. 6k–m), implying more extensive disruption of PDIM(+) growth in this detergent. The odd-chain fatty acid valerate also restored PDIM(+) growth, but not the even-chain fatty acids acetate or butyrate, or the three-carbon metabolite pyruvate (Extended Data Fig. 6g–j), demonstrating this effect is specific to propionyl-CoA generating carbon sources. Similar to vancomycin resistance assays, we again did not observe a comparable effect with leucine supplementation (Supplementary Fig. 4), suggesting that at this concentration leucine is preferably routed into anabolic pathways rather than catabolised as a source of propionyl-CoA. Supplementing with cholesterol not only restored PDIM(+) growth but also significantly reduced the growth of PDIM(-) *Mtb* (Fig. 3e). The growth reduction of PDIM(-) *Mtb* is likely related to the reduced ability to maintain redox homeostasis via lipid anabolism[36], a mechanism induced during cholesterol catabolism[37]. Taken together, these data indicate that in standard media PDIM(+) growth is impaired due to a deficiency of MMCoA. This was supported by measuring the intracellular abundance of MMCoA by LC-MS. In unsupplemented media, MMCoA levels in PDIM(+) *Mtb* were approximately 3-fold lower than in PDIM(-), but increased to similar levels with propionate supplementation (Fig. 3f). Vitamin B_{12} supplementation also significantly increased MMCoA but not propionyl-CoA levels in PDIM(+) *Mtb* (Fig. 3g and Extended Data Fig. 7a), supporting the notion that MMCoA deficiency specifically is responsible for the growth retardation in PDIM(+) *Mtb.*

Propionate and vitamin B_{12} maintain an intact PDIM biosynthetic pathway

Based on these findings, we reasoned that addition of propionate to culture media would prevent PDIM loss by eliminating the growth advantage of PDIM(-) cells. Whilst arguably

cholesterol could also be used for this purpose, propionate is both more affordable and much simpler to work with as a routine media supplement. To assess this, we performed *in vitro* experimental evolution using culture stocks with different PDIM(+) to PDIM(-) ratios. First, we serially passaged H37Rv-B – a moderately PDIM(+) mixed population (Fig. 2f), by weekly subculture in 7H9/OADC/glycerol/tyloxapol ± 0.1 or 1.0 mM propionate and assessed PDIM levels by TLC and VAN10-P assays. Considerable PDIM loss was observed in unsupplemented media whereas propionate supplementation fully maintained PDIM production (Fig. 4a). Repeating this experiment but starting from a PDIM(+) clone, we saw a marked decline in PDIM in unsupplemented media after five passages, whilst 0.1 mM propionate maintained PDIM production for the duration of the experiment (Extended Data Fig. 8c). Strikingly, starting from H37Rv-A – a predominantly PDIM(-) population, PDIM levels progressively increased with propionate (Fig. 4b). VAN10-P screening of single colonies confirmed enrichment of PDIM(+) clones (Fig. 4c), demonstrating 0.1 mM propionate positively selects for PDIM-producing *Mtb*. We speculated that whilst advantageous for the growth of PDIM(+) *Mtb*, 0.1 mM propionate selects against PDIM(-) cells due to propionyl-CoA toxicity[38] in the absence of a functional PDIM biosynthetic pathway. Indeed, the addition of vitamin B_{12} to alleviate propionyl-CoA toxicity via activation of the methylmalonyl pathway[22,35] considerably slowed the selection process and resembled more cultures with vitamin B_{12} alone (Fig. 4d and Extended Data Fig. 8d,e). This represents an important advance for the tuberculosis field as it demonstrates that propionate improves the growth of PDIM(+) cells and provides a competitive advantage against spontaneous PDIM(-) mutants, thereby enabling the maintenance of pure PDIM(+) *Mtb* cultures *in vitro*.

Propionate increases rifampicin and bedaquiline resistance via enhanced PDIM production

Propionate provides a source of MMCoA precursors that mimics host nutrient conditions but are classically absent in *Mtb* culture media. As PDIM levels had such a profound effect on vancomycin resistance, we sought to further explore the impact of propionate supplementation on drug resistance. MIC assays of several first and second line antitubercular drugs revealed that propionate significantly increased resistance to rifampicin and bedaquiline in a PDIM-dependent manner, while smaller inhibitors like isoniazid, linezolid, and pretomanid showed no difference (Fig. 5 and Supplementary Figs. 5 and 6). Vitamin B_{12} mirrored the effects of propionate supplementation on rifampicin and bedaquiline resistance (Fig. 5a,c), consistent with enhanced resistance due to increased PDIM production. Notably, the rifampicin MIC_{90} for PDIM(+) *Mtb* in propionate-supplemented media reduced ~30-fold when tyloxapol was replaced with Tween 80 (Fig. 6), arguing that Tween 80 is unsuitable for detecting *in vivo* relevant drug sensitivity. These data are also congruent with our earlier results showing greater resistance of PDIM(+) *Mtb* to large compounds and lower permeability compared to PDIM(-) (Extended Data Fig. 1). One outlier to this trend was capreomycin (668.7 g/mol), which did not exhibit a PDIM-propionate MIC shift (Supplementary Fig. 5a). Wang *et al*. have also reported PDIM-dependent resistance to the small molecule inhibitor 3bMP1 (229.3 g/mol)[12], indicating that the relationship between the PDIM permeability barrier and drug uptake is complex though the uptake of large compounds is more likely to be affected by PDIM.

Discussion

The mycobacterial cell wall plays a crucial role in the interactions between the pathogen and host[39]. However, the study of *Mtb* cell wall biology and pathogenesis has long been impeded by PDIM bias. It has been nearly 50 years since the first report associating PDIM loss with virulence attenuation *in vivo*[8] and over 20 years since PDIM loss and attenuation were linked at the genetic

level[6,7]. Numerous studies have since been published reporting spontaneous PDIM loss not only in *Mtb* H37Rv[3-5,12], but also in *Mtb* Erdman[40], HN878[3], CDC1551[29,41], and in *M. bovis* BCG vaccine strains[42]. The PDIM problem is thus both long-standing and far-reaching, and the number of studies unpublished due to PDIM bias and the time and resources spent chasing PDIM-related phenotypes are high.

We discovered that the cause and solution of the PDIM problem are rooted in *Mtb* metabolism. *Mtb* growth is impaired in the absence of an exogenous source of MMCoA precursors, providing a selection pressure for PDIM loss. This bottleneck can be alleviated by supplementing propionyl-CoA-generating carbon sources such as odd-chain fatty acids or cholesterol, or the cofactor vitamin B_{12}, which increase MMCoA pools and restore full growth of PDIM(+) *Mtb*. The affinity of *Mtb* for host fatty acids was first described by Segal and Bloch in 1956[43] and today we know that *Mtb* is a specialist in cholesterol utilization[18]. Cholesterol is thought to be a major source of propionyl-CoA in the host[19], and *Mtb* has evolved to efficiently use this host-derived resource as fuel for cellular metabolism and a building block for virulence lipids[18,35]. Moreover, starving the bacterium of propionyl-CoA via cholesterol limitation improves macrophage control of *Mtb*[44], demonstrating a crucial role for this metabolite in *Mtb* during infection. Why then, to this day, has *Mtb* culture media remained devoid of propionyl-CoA precursors? Most *Mtb* culture media were optimized to promote rapid planktonic growth rather than to reflect the nutrient environment found in the host[45,46], and we speculate the toxicity of high concentrations of odd-chain fatty acids has previously discouraged their inclusion. Contrary to its negative reputation, we show that 0.1 mM propionate is in fact advantageous for PDIM(+) growth and selects against PDIM(-) cells analogous to animal passage, providing an elegant and long-sought solution to the PDIM problem. Our data also clearly demonstrate that tyloxapol and not Tween 80 should be used in PDIM assays

and PDIM selective media as tyloxapol maintains PDIM-dependent impermeability, whilst Tween 80 strips PDIM and other cell wall components[27].

These data also have ramifications for future drug discovery efforts. During host infection, *Mtb* survives in a PDIM-rich state[17], however, PDIM production is poorly supported in current culture media potentially leading to overestimation of drug potency. Indeed, we show that PDIM levels affect the potency of rifampicin, bedaquiline and other high molecular weight inhibitors. In concert with the current literature[47,48], this clearly points to the mycobacterial cell wall as an important factor in drug efficacy. In addition, the tremendous increase in vancomycin and rifampicin sensitivity with Tween 80, together with previous reports of this phenomenon[49,50], strongly advocate for the use of tyloxapol to maintain the natural permeability barrier in *Mtb*. Our findings also expand on previous observations associating propionyl-CoA metabolism with rifampicin resistance[25,47] by directly linking propionyl-CoA and PDIM production with enhanced rifampicin resistance. The decreased virulence and increased drug sensitivity of PDIM(-) *Mtb* suggest that inhibitors of PDIM biosynthesis could significantly increase the *in vivo* potency of current drug regimens. Such a therapeutic option would be highly specific, as PDIMs are confined to slow-growing, pathogenic mycobacteria. Furthermore, inhibitors targeting propionyl-CoA metabolism could be synergistic with rifampicin due to downstream effects on PDIM.

The main recommendations stemming from our study are to routinely supplement culture media with 0.1 mM propionate and avoid Tween 80 to prevent PDIM loss and the emergence of heterogeneous populations whilst simultaneously augmenting PDIM production. VAN-P assays provide the tools for routine strain testing during genetic manipulations and enable efficient re-isolation of PDIM(+) strains from mixed populations. Pure and properly maintained PDIM(+) strains will be indispensable for studying interactions with host immunity, as well as for high-

266 stakes pre-clinical work such as vaccine studies in non-human primates. Moreover, today in the
267 emerging era of *Mtb* systems biology where large pools of genetically modified strains are crucial
268 tools for *in vitro* and *in vivo* studies[51-53], preventing secondary PDIM mutations is imperative.
269 Importantly, our approach is accessible to everyone, including labs in low-resource settings.

270 Taken together, our discoveries not only solve the PDIM problem, but also highlight how
271 the host nutritional environment has shaped the close coupling between *Mtb* metabolism and its
272 virulence. Our findings exemplify how discrepancies between the host and *in vitro* nutrient
273 environment can attenuate bacterial pathogenicity and provide essential tools and culture
274 conditions to finally eliminate the PDIM problem from tuberculosis research.

References

1 Daffe, M. & Laneelle, M. A. Distribution of phthiocerol diester, phenolic mycosides and related compounds in mycobacteria. *J Gen Microbiol* **134**, 2049-2055 (1988). https://doi.org:10.1099/00221287-134-7-2049

2 Rens, C., Chao, J. D., Sexton, D. L., Tocheva, E. I. & Av-Gay, Y. Roles for phthiocerol dimycocerosate lipids in Mycobacterium tuberculosis pathogenesis. *Microbiology (Reading)* **167** (2021). https://doi.org:10.1099/mic.0.001042

3 Domenech, P. & Reed, M. B. Rapid and spontaneous loss of phthiocerol dimycocerosate (PDIM) from Mycobacterium tuberculosis grown in vitro: implications for virulence studies. *Microbiology (Reading)* **155**, 3532-3543 (2009). https://doi.org:10.1099/mic.0.029199-0

4 Manjunatha, U. H. *et al.* Identification of a nitroimidazo-oxazine-specific protein involved in PA-824 resistance in Mycobacterium tuberculosis. *Proc Natl Acad Sci U S A* **103**, 431-436 (2006). https://doi.org:10.1073/pnas.0508392103

5 Kirksey, M. A. *et al.* Spontaneous phthiocerol dimycocerosate-deficient variants of Mycobacterium tuberculosis are susceptible to gamma interferon-mediated immunity. *Infect Immun* **79**, 2829-2838 (2011). https://doi.org:10.1128/IAI.00097-11

6 Cox, J. S., Chen, B., McNeil, M. & Jacobs, W. R., Jr. Complex lipid determines tissue-specific replication of Mycobacterium tuberculosis in mice. *Nature* **402**, 79-83 (1999). https://doi.org:10.1038/47042

7 Camacho, L. R., Ensergueix, D., Perez, E., Gicquel, B. & Guilhot, C. Identification of a virulence gene cluster of Mycobacterium tuberculosis by signature-tagged transposon

297 mutagenesis. *Mol Microbiol* **34**, 257-267 (1999). https://doi.org:10.1046/j.1365-
298 2958.1999.01593.x
299 8 Goren, M. B., Brokl, O. & Schaefer, W. B. Lipids of putative relevance to virulence in
300 Mycobacterium tuberculosis: phthiocerol dimycocerosate and the attenuation indicator
301 lipid. *Infect Immun* **9**, 150-158 (1974). https://doi.org:10.1128/iai.9.1.150-158.1974
302 9 Murry, J. P., Pandey, A. K., Sassetti, C. M. & Rubin, E. J. Phthiocerol dimycocerosate
303 transport is required for resisting interferon-gamma-independent immunity. *J Infect Dis*
304 **200**, 774-782 (2009). https://doi.org:10.1086/605128
305 10 Day, T. A. *et al.* Mycobacterium tuberculosis strains lacking surface lipid phthiocerol
306 dimycocerosate are susceptible to killing by an early innate host response. *Infect Immun*
307 **82**, 5214-5222 (2014). https://doi.org:10.1128/IAI.01340-13
308 11 Rousseau, C. *et al.* Production of phthiocerol dimycocerosates protects Mycobacterium
309 tuberculosis from the cidal activity of reactive nitrogen intermediates produced by
310 macrophages and modulates the early immune response to infection. *Cell Microbiol* **6**, 277-
311 287 (2004). https://doi.org:10.1046/j.1462-5822.2004.00368.x
312 12 Wang, Q. *et al.* PE/PPE proteins mediate nutrient transport across the outer membrane of
313 Mycobacterium tuberculosis. *Science* **367**, 1147-1151 (2020).
314 https://doi.org:10.1126/science.aav5912
315 13 Camacho, L. R. *et al.* Analysis of the phthiocerol dimycocerosate locus of Mycobacterium
316 tuberculosis. Evidence that this lipid is involved in the cell wall permeability barrier. *J Biol*
317 *Chem* **276**, 19845-19854 (2001). https://doi.org:10.1074/jbc.M100662200
318 14 Tran, V., Ahn, S. K., Ng, M., Li, M. & Liu, J. Loss of Lipid Virulence Factors Reduces the
319 Efficacy of the BCG Vaccine. *Sci Rep* **6**, 29076 (2016). https://doi.org:10.1038/srep29076

15 Soetaert, K. *et al.* Increased Vancomycin Susceptibility in Mycobacteria: a New Approach To Identify Synergistic Activity against Multidrug-Resistant Mycobacteria. *Antimicrob Agents Chemother* **59**, 5057-5060 (2015). https://doi.org:10.1128/AAC.04856-14

16 Rodrigues, L., Viveiros, M. & Ainsa, J. A. Measuring efflux and permeability in mycobacteria. *Methods Mol Biol* **1285**, 227-239 (2015). https://doi.org:10.1007/978-1-4939-2450-9_13

17 Jain, M. *et al.* Lipidomics reveals control of Mycobacterium tuberculosis virulence lipids via metabolic coupling. *Proc Natl Acad Sci U S A* **104**, 5133-5138 (2007). https://doi.org:10.1073/pnas.0610634104

18 Pandey, A. K. & Sassetti, C. M. Mycobacterial persistence requires the utilization of host cholesterol. *Proc Natl Acad Sci U S A* **105**, 4376-4380 (2008). https://doi.org:10.1073/pnas.0711159105

19 Griffin, J. E. *et al.* Cholesterol catabolism by Mycobacterium tuberculosis requires transcriptional and metabolic adaptations. *Chem Biol* **19**, 218-227 (2012). https://doi.org:10.1016/j.chembiol.2011.12.016

20 Gopinath, K., Moosa, A., Mizrahi, V. & Warner, D. F. Vitamin B12 metabolism in Mycobacterium tuberculosis. *Future Microbiol* **8**, 1405-1418 (2013). https://doi.org:10.2217/fmb.13.113

21 Gopinath, K. *et al.* A vitamin B12 transporter in Mycobacterium tuberculosis. *Open Biol* **3**, 120175 (2013). https://doi.org:10.1098/rsob.120175

22 Savvi, S. *et al.* Functional characterization of a vitamin B12-dependent methylmalonyl pathway in Mycobacterium tuberculosis: implications for propionate metabolism during

growth on fatty acids. *J Bacteriol* **190**, 3886-3895 (2008). https://doi.org:10.1128/JB.01767-07

23 Yang, X., Nesbitt, N. M., Dubnau, E., Smith, I. & Sampson, N. S. Cholesterol metabolism increases the metabolic pool of propionate in Mycobacterium tuberculosis. *Biochemistry* **48**, 3819-3821 (2009). https://doi.org:10.1021/bi9005418

24 Quinonez, C. G. *et al.* The Role of Fatty Acid Metabolism in Drug Tolerance of Mycobacterium tuberculosis. *mBio* **13**, e0355921 (2022). https://doi.org:10.1128/mbio.03559-21

25 Hicks, N. D. *et al.* Clinically prevalent mutations in Mycobacterium tuberculosis alter propionate metabolism and mediate multidrug tolerance. *Nat Microbiol* **3**, 1032-1042 (2018). https://doi.org:10.1038/s41564-018-0218-3

26 Massey, L. K., Sokatch, J. R. & Conrad, R. S. Branched-chain amino acid catabolism in bacteria. *Bacteriol Rev* **40**, 42-54 (1976). https://doi.org:10.1128/br.40.1.42-54.1976

27 Ortalo-Magne, A. *et al.* Identification of the surface-exposed lipids on the cell envelopes of Mycobacterium tuberculosis and other mycobacterial species. *J Bacteriol* **178**, 456-461 (1996). https://doi.org:10.1128/jb.178.2.456-461.1996

28 Jain, P. *et al.* Specialized transduction designed for precise high-throughput unmarked deletions in Mycobacterium tuberculosis. *mBio* **5**, e01245-01214 (2014). https://doi.org:10.1128/mBio.01245-14

29 Dechow, S. J., Baker, J. J., Murto, M. & Abramovitch, R. B. ppe51 Variants Enable Growth of Mycobacterium tuberculosis at Acidic pH by Selectively Promoting Glycerol Uptake. *J Bacteriol*, e0021222 (2022). https://doi.org:10.1128/jb.00212-22

30 Gopal, P. *et al.* Pyrazinamide Resistance Is Caused by Two Distinct Mechanisms: Prevention of Coenzyme A Depletion and Loss of Virulence Factor Synthesis. *ACS Infect Dis* **2**, 616-626 (2016). https://doi.org:10.1021/acsinfecdis.6b00070

31 Orsi, R. H., Bowen, B. M. & Wiedmann, M. Homopolymeric tracts represent a general regulatory mechanism in prokaryotes. *BMC Genomics* **11**, 102 (2010). https://doi.org:10.1186/1471-2164-11-102

32 Mizrahi, V. & Andersen, S. J. DNA repair in Mycobacterium tuberculosis. What have we learnt from the genome sequence? *Mol Microbiol* **29**, 1331-1339 (1998). https://doi.org:10.1046/j.1365-2958.1998.01038.x

33 Dolan, S. K. *et al.* Loving the poison: the methylcitrate cycle and bacterial pathogenesis. *Microbiology (Reading)* **164**, 251-259 (2018). https://doi.org:10.1099/mic.0.000604

34 Munoz-Elias, E. J., Upton, A. M., Cherian, J. & McKinney, J. D. Role of the methylcitrate cycle in Mycobacterium tuberculosis metabolism, intracellular growth, and virulence. *Mol Microbiol* **60**, 1109-1122 (2006). https://doi.org:10.1111/j.1365-2958.2006.05155.x

35 Lee, W., VanderVen, B. C., Fahey, R. J. & Russell, D. G. Intracellular Mycobacterium tuberculosis exploits host-derived fatty acids to limit metabolic stress. *J Biol Chem* **288**, 6788-6800 (2013). https://doi.org:10.1074/jbc.M112.445056

36 Singh, A. *et al.* Mycobacterium tuberculosis WhiB3 maintains redox homeostasis by regulating virulence lipid anabolism to modulate macrophage response. *PLoS Pathog* **5**, e1000545 (2009). https://doi.org:10.1371/journal.ppat.1000545

37 Lu, R. *et al.* Catabolism of the Cholesterol Side Chain in Mycobacterium tuberculosis Is Controlled by a Redox-Sensitive Thiol Switch. *ACS Infect Dis* **3**, 666-675 (2017). https://doi.org:10.1021/acsinfecdis.7b00072

38 Eoh, H. & Rhee, K. Y. Methylcitrate cycle defines the bactericidal essentiality of isocitrate lyase for survival of Mycobacterium tuberculosis on fatty acids. *Proc Natl Acad Sci U S A* **111**, 4976-4981 (2014). https://doi.org:10.1073/pnas.1400390111

39 Dulberger, C. L., Rubin, E. J. & Boutte, C. C. The mycobacterial cell envelope - a moving target. *Nat Rev Microbiol* **18**, 47-59 (2020). https://doi.org:10.1038/s41579-019-0273-7

40 Marrero, J., Rhee, K. Y., Schnappinger, D., Pethe, K. & Ehrt, S. Gluconeogenic carbon flow of tricarboxylic acid cycle intermediates is critical for Mycobacterium tuberculosis to establish and maintain infection. *Proc Natl Acad Sci U S A* **107**, 9819-9824 (2010). https://doi.org:10.1073/pnas.1000715107

41 Maksymiuk, C. *et al.* Comparison of transposon and deletion mutants in Mycobacterium tuberculosis: The case of rv1248c, encoding 2-hydroxy-3-oxoadipate synthase. *Tuberculosis (Edinb)* **95**, 689-694 (2015). https://doi.org:10.1016/j.tube.2015.08.009

42 Chen, J. M., Islam, S. T., Ren, H. & Liu, J. Differential productions of lipid virulence factors among BCG vaccine strains and implications on BCG safety. *Vaccine* **25**, 8114-8122 (2007). https://doi.org:10.1016/j.vaccine.2007.09.041

43 Bloch, H. & Segal, W. Biochemical differentiation of Mycobacterium tuberculosis grown in vivo and in vitro. *J Bacteriol* **72**, 132-141 (1956). https://doi.org:10.1128/jb.72.2.132-141.1956

44 Babunovic, G. H. *et al.* CRISPR Interference Reveals That All-Trans-Retinoic Acid Promotes Macrophage Control of Mycobacterium tuberculosis by Limiting Bacterial Access to Cholesterol and Propionyl Coenzyme A. *mBio* **13**, e0368321 (2022). https://doi.org:10.1128/mbio.03683-21

45 Dubos, R. J. & Middlebrook, G. Media for tubercle bacilli. *Am Rev Tuberc* **56**, 334-345 (1947).

46 Dubos, R. J. Rapid and submerged growth of mycobacteria in liquid media. *Proc Soc Exp Biol Med* **58**, 361-362 (1945).

47 Koh, E. I. *et al.* Chemical-genetic interaction mapping links carbon metabolism and cell wall structure to tuberculosis drug efficacy. *Proc Natl Acad Sci U S A* **119**, e2201632119 (2022). https://doi.org:10.1073/pnas.2201632119

48 Li, S. *et al.* CRISPRi chemical genetics and comparative genomics identify genes mediating drug potency in Mycobacterium tuberculosis. *Nat Microbiol* **7**, 766-779 (2022). https://doi.org:10.1038/s41564-022-01130-y

49 Chengalroyen, M. D. *et al.* DNA-Dependent Binding of Nargenicin to DnaE1 Inhibits Replication in Mycobacterium tuberculosis. *ACS Infect Dis* **8**, 612-625 (2022). https://doi.org:10.1021/acsinfecdis.1c00643

50 Wang, Q. & Boshoff, H. I. M. Determining Minimum Inhibitory Concentrations in Liquid Cultures or on Solid Medium. *Methods Mol Biol* **2314**, 595-609 (2021). https://doi.org:10.1007/978-1-0716-1460-0_26

51 DeJesus, M. A. *et al.* Comprehensive Essentiality Analysis of the Mycobacterium tuberculosis Genome via Saturating Transposon Mutagenesis. *mBio* **8** (2017). https://doi.org:10.1128/mBio.02133-16

52 Bosch, B. *et al.* Genome-wide gene expression tuning reveals diverse vulnerabilities of M. tuberculosis. *Cell* **184**, 4579-4592 e4524 (2021). https://doi.org:10.1016/j.cell.2021.06.033

53 Zhang, Y. J. *et al.* Tryptophan biosynthesis protects mycobacteria from CD4 T-cell-mediated killing. *Cell* **155**, 1296-1308 (2013). https://doi.org:10.1016/j.cell.2013.10.045

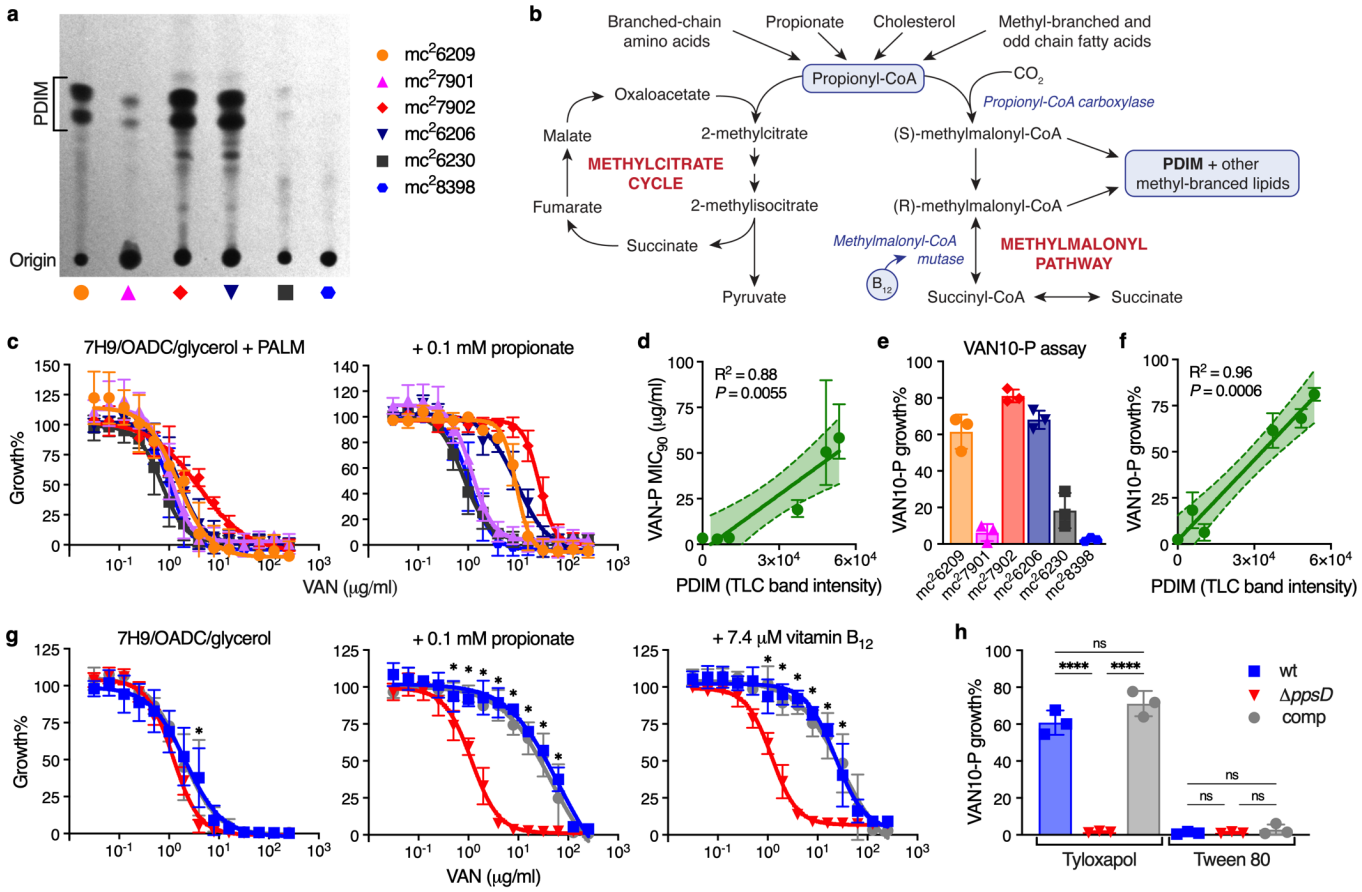

Fig. 1 | Vancomycin resistance is enhanced by propionate or vitamin B_{12} supplementation and is predictive of PDIM production in *Mtb*. **a**, TLC lipid analysis of the PDIM reference strain set (see Supplementary Table 1). **b**, Metabolic pathways of methylmalonyl-CoA production and propionyl-CoA catabolism. **c**, Vancomycin resistance of the *Mtb* PDIM reference strain set in 7H9/OADC/glycerol/tyloxapol + PALM (pantothenate, arginine, leucine, and methionine) media, and additionally supplemented with 0.1 mM propionate ('VAN-P' MIC), measured after 7 days incubation. **d**, Correlation between VAN-P MIC_{90} ± 95% CI from the curve fit in (**c**) (+ 0.1 mM propionate) and PDIM band intensity from (**a**). The band represents the 95% CI. **e**, 'VAN10-P' assay comparing growth in 10 μg/ml vancomycin with 0.1 mM propionate to drug-free controls (VAN10 OD / VAN0 OD × 100 = VAN10 growth%). **f**, Correlation between VAN10-P growth%

from (**e**) and PDIM from (**a**). **g**, Vancomycin resistance of isogenic PDIM(+) and PDIM(-) *Mtb* H37Rv strains in standard 7H9/OADC/glycerol/tyloxapol media and supplemented with 0.1 mM propionate or 7.4 μM vitamin B_{12} (10 μg/ml). *$P < 0.001$ for both wt and comp versus Δ*ppsD*; two-way ANOVA with Tukey's multiple comparison test. **h**, VAN10-P assay of H37Rv strains with tyloxapol or Tween 80. ****$P < 0.0001$; one-way ANOVA with Tukey's multiple comparison test. MIC data show mean ± SD for $n = 4$ biological replicates from two independent experiments. VAN10-P data show mean ± SD for $n = 3$ three independent experiments, each performed in triplicate.

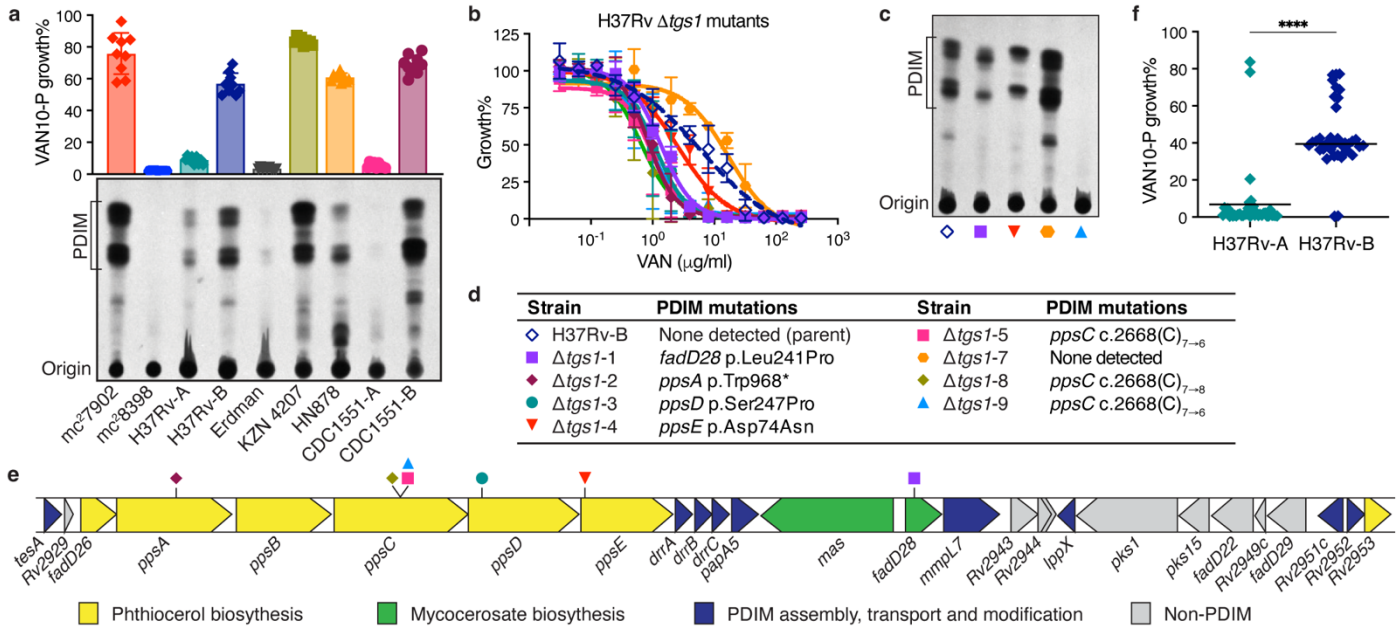

451

452 **Fig. 2 | VAN-P assays accurately predict PDIM status during genetic manipulations and**
453 **across different *Mtb* strains and lineages. a**, TLC lipid analysis and VAN10-P assays of different
454 laboratory stocks of virulent *Mtb* strains alongside *Mtb* mc²7902 and mc²8398. Mean ± SD for
455 $n = 9$ pairwise comparisons between triplicate wells. **b**, VAN-P MIC assays of eight Δ*tgs1* mutants
456 and the parent H37Rv-B. Mean ± SD for $n = 3$–4 biological replicates from two independent
457 experiments. **c**, TLC lipid analysis of four Δ*tgs1* mutants and H37Rv-B. Lipid extracts in (**a**) and
458 (**c**) were run on the same TLC plate. **d**, Mutations in PDIM biosynthetic genes of Δ*tgs1* mutants
459 (see also Extended Data Fig. 5). **e**, Schematic showing the PDIM gene cluster and location of
460 secondary PDIM mutations in Δ*tgs1* mutants. **f**, VAN10-P screening of single colonies isolated
461 from H37Rv-A ($n = 38$) and H37Rv-B ($n = 37$). Each colony was assayed in triplicate and data
462 points represent mean VAN10-P growth%. Lines indicate the median. ****$P < 0.0001$; unpaired
463 two-tailed Mann-Whitney test.

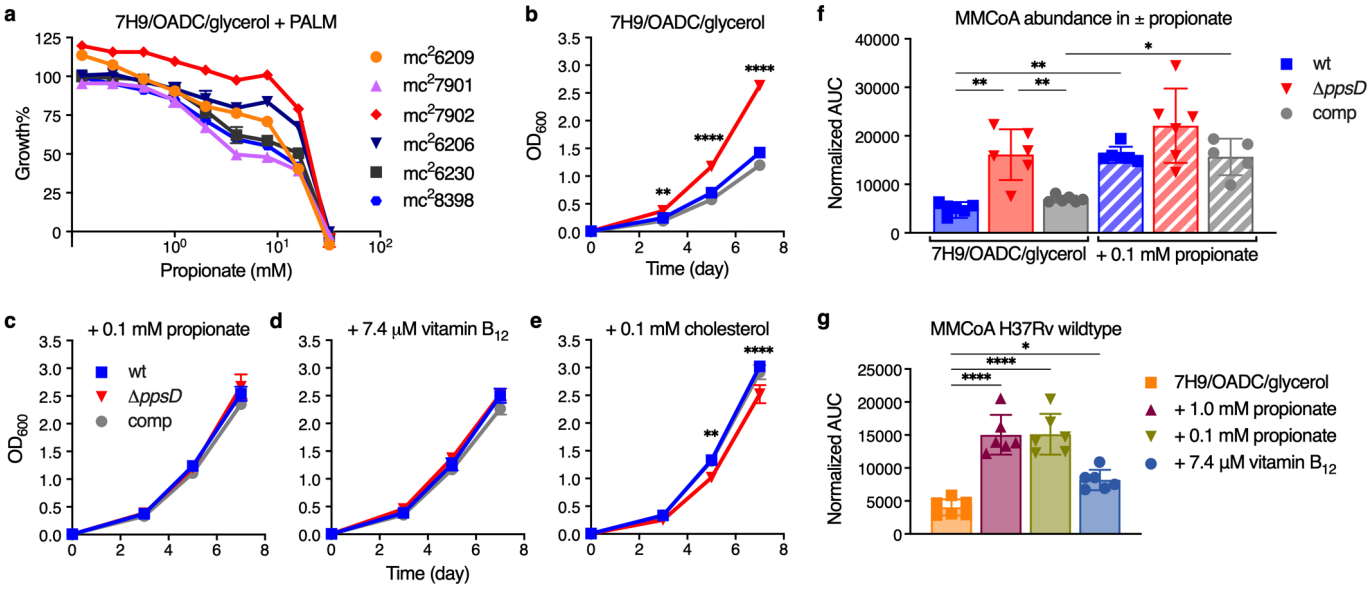

464

465 **Fig. 3 | Propionate and vitamin B_{12} supplementation restore the growth of PDIM(+) *Mtb*. a**,
466 Relative growth of the PDIM reference strain set in 7H9/OADC/glycerol/tyloxapol + PALM
467 media with increasing concentrations of propionate compared to no propionate controls. Mean ±
468 SD for $n = 3$ biological replicates. **b**–**e**, Growth curves of PDIM(+) and PDIM(-) *Mtb* H37Rv in
469 (**b**) standard 7H9/OADC/glycerol/tyloxapol and (**c**) supplemented with 0.1 mM propionate, (**d**)
470 7.4 μM vitamin B_{12} (10 μg/ml), or (**e**) 0.1 mM cholesterol. Mean ± SD for $n = 3$ biological
471 replicates. $^{**}P < 0.01$, $^{***}P < 0.001$, $^{****}P < 0.0001$ for both wt and comp versus Δ*ppsD*;
472 two-way ANOVA with Šidák's multiple comparison test. Data in (**a**–**e**) are representative of at
473 least two independent experiments. For some data points the SD is smaller than the data symbols.
474 **f**, Abundance of methylmalonyl-CoA (MMCoA) in PDIM(+) and PDIM(-) H37Rv grown in
475 standard 7H9/OADC/glycerol/tyloxapol media ± 0.1 mM propionate, and **g**, PDIM(+) H37Rv
476 wildtype in standard media and supplemented with either propionate or vitamin B_{12}. Abundances
477 are shown as normalized area under the curve (AUC). Mean ± SD for $n = 6$ biological replicates
478 from two independent experiments. $^{*}P < 0.05$, $^{**}P < 0.01$, $^{****}P < 0.0001$; one-way ANOVA

479 with Tukey's multiple comparison test. Significant differences between ± propionate for each
480 strain and between strains for each condition are indicated in (**f**), and compared to unsupplemented
481 media in (**g**).

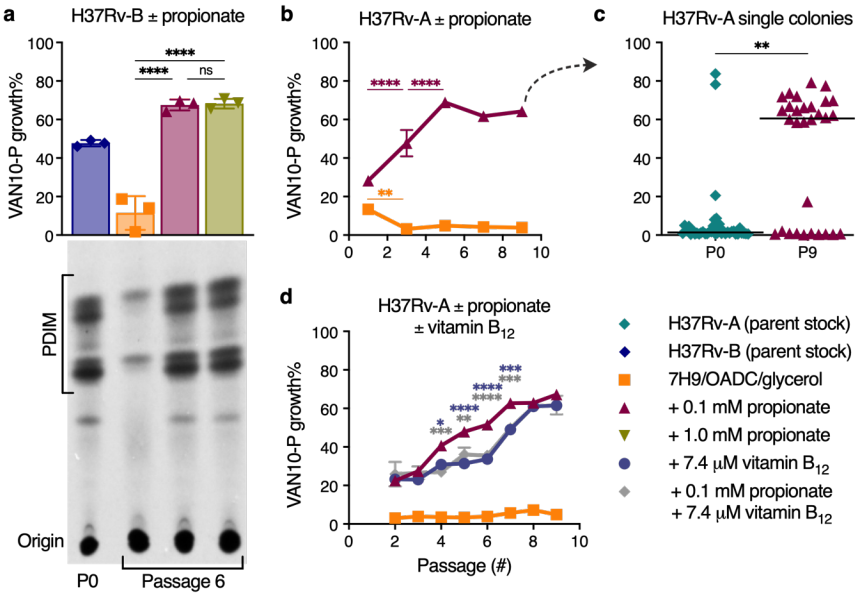

482

483 **Fig. 4 | Propionate and vitamin B_{12} supplementation prevent PDIM loss in *Mtb*.** **a**, VAN10-P
484 and TLC lipid analysis of PDIM levels in *Mtb* H37Rv-B following serial passage in
485 7H9/OADC/glycerol/tyloxapol media ± 0.1 or 1.0 mM propionate. ****$P < 0.0001$; one-way
486 ANOVA with Tukey's multiple comparison test. A representative result is shown for one of two
487 biological replicates analysed by TLC (see also Extended Data Fig. 8b). **b**, VAN10-P assays of
488 H37Rv-A passaged in ± 0.1 mM propionate. **c**, VAN10-P screening of single colonies of H37Rv-A
489 before ($n = 38$; same data as Fig. 2f) and after propionate passage in (**b**) ($n = 30$). Each colony was
490 assayed in triplicate and data points represent mean VAN10-P growth%. Lines indicate the
491 median. $P = 0.0047$; unpaired two-tailed Mann-Whitney test. **d**, VAN10-P assays of H37Rv-A
492 passaged in media supplemented with ± 0.1 mM propionate and 7.4 μM vitamin B_{12} (10 μg/ml)
493 alone and in combination. For (**b**,**d**) *$P < 0.05$, **$P < 0.01$, ***$P < 0.001$, ****$P < 0.0001$; two-
494 way ANOVA with Tukey's multiple comparison test. Significant differences are indicated
495 between successive timepoints for each condition in (**b**) and compared to + 0.1 mM propionate in
496 (**d**). $P > 0.05$ for vitamin B_{12} versus vitamin B_{12} + propionate and ****$P < 0.0001$ for standard

media versus each supplemented condition at all timepoints in (**d**). VAN10-P data in (**a**,**b**,**d**) show mean ± SD for $n = 3$ biological replicates, each assayed in triplicate. For some data points the SD is smaller than the data symbols.

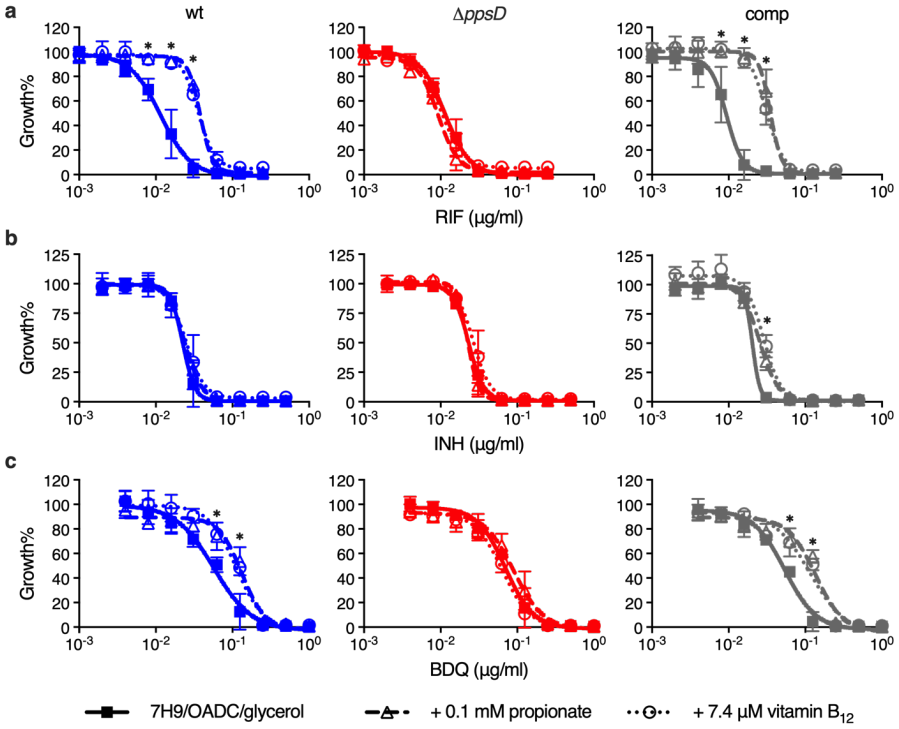

Fig. 5 | Propionate and vitamin B_{12} supplementation increase rifampicin and bedaquiline resistance of *Mtb* in a PDIM-dependent manner. a, Sensitivity of PDIM(+) and PDIM(-) *Mtb* H37Rv to rifampicin (RIF), **b**, bedaquiline (BDQ), and **c**, isoniazid (INH), in standard 7H9/OADC/glycerol/tyloxapol media and supplemented with either 0.1 mM propionate or 7.4 μM vitamin B_{12} (10 μg/ml). *$P < 0.001$ for both propionate and vitamin B_{12} versus unsupplemented; two-way ANOVA with Tukey's multiple comparison test. Mean ± SD for $n = 4$ biological replicates from two independent experiments.

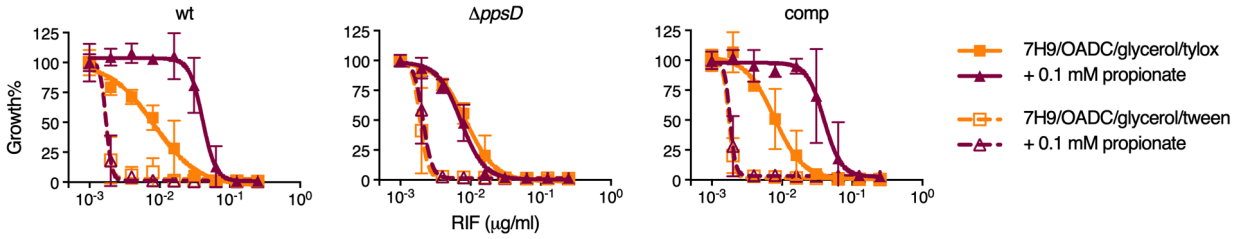

508

509 **Fig. 6 | Tween 80 increases the sensitivity of *Mtb* to rifampicin and abolishes PDIM-**
510 **dependent differences in MIC.** Sensitivity of PDIM(+) and PDIM(-) *Mtb* H37Rv to rifampicin
511 (RIF) in 7H9/OADC/glycerol ± 0.1 mM propionate using either tyloxapol or Tween 80 as the
512 culture detergent. Mean ± SD for $n = 4$ biological replicates from two independent experiments.

Methods

Bacterial strains, culture condition and reagents

Mtb strains were obtained from laboratory stocks and are listed in Supplementary Tables 1 and 2. Fresh starter cultures were inoculated from frozen seed stocks and then subcultured once before use in experiments. Subcultures were typically grown for four days to an optical density (OD) at 600 nm (OD_{600}) of ~0.8. For BSL2 strains, OD_{600} was measured using a GENESYS 140 spectrophotometer (Thermo Fisher Scientific). For BSL3 strains, OD_{600} was measured on a Biowave WPA CO8000 spectrophotometer (Biochrom Ltd.) and then converted using a calibration curve constructed against a GENESYS 10uv spectrophotometer (Thermo Fisher Scientific). Preculturing steps were performed using Middlebrook 7H9 broth supplemented with 10% (v/v) OADC (0.6 g/l sodium oleate, 50 g/l bovine serum albumin fraction V, 20 g/l dextrose, 40 mg/l catalase, 8.5 g/l sodium chloride), 0.2% (v/v) glycerol, and 0.05% (v/v) tyloxapol. This is referred to as standard 7H9/OADC/glycerol/tyloxapol media. BSL2 strains (Supplementary Table 1) were additionally supplemented with 24 mg/l D-calcium pantothenate, 200 mg/l L-arginine, 50 mg/l L-leucine, and 50 mg/l L-methionine ('PALM' supplements). Hygromycin B at 75 µg/ml and kanamycin at 30 µg/ml were added to precultures as indicated (Supplementary Table 2). For supplemented media, 1000 × supplement stocks were prepared in MilliQ water, filter sterilized, then added to standard media and the pH checked. Final supplement concentrations were as follows: 0.1 mM or 1.0 mM sodium propionate, 7.4 µM vitamin B_{12} (10 µg/ml), and 0.1 mM sodium pyruvate, sodium acetate, sodium butyrate and valeric acid. Cholesterol was prepared at 0.1 M in 1:1 (v/v) EtOH/tyloxapol as previously described[35] and then added to detergent-free media to give a final concentration of 0.1 mM cholesterol and 0.05% tyloxapol. Controls were prepared by adding EtOH/tyloxapol in the same manner to provide the detergent. For Tween 80

experiments, 0.05% Tween 80 was used in place of tyloxapol. For growth curve experiments, triplicate inkwells with 5 ml of media were inoculated at a starting OD_{600} of 0.01. Broth cultures were grown at 37 ºC with gentle shaking (100 rpm for BSL2 strains, 80 rpm for BSL3). Middlebrook 7H10 agar supplemented with 10% (v/v) OADC and 0.5% (v/v) glycerol (7H10/OADC/glycerol) was used as a solid media for plating and plates were incubated at 37 ºC for three weeks. Supplier information for media components and supplements are listed in Supplementary Table 3.

Mutant generation and complementation

Deletion of the *tgs1* (*Rv3130c*), *ppsD* (*Rv2934*) and *mas* (*Rv2940c*) genes was carried out by specialized transduction as previously described[28]. H37Rv-B was used to generate H37Rv Δ*tgs1* mutants; H37Rv-SC [a single PDIM(+) clone isolated from H37Rv-B by VAN10-P screening] was used to generate H37Rv Δ*ppsD*; and CDC1551-B to generate CDC1551 Δ*mas* (Supplementary Table 2). Transductants were selected on plates containing hygromycin (75 μg/ml) and the deletion was confirmed by 3-primer PCR and whole genome sequencing (WGS). The Δ*ppsD* strain was complemented using the integrative vector pMV361[54] containing a copy of the *ppsD* gene under control of the HSP60 promoter (pMV361-*ppsD*). The complementation plasmid was constructed by Gibson assembly using the NEBuilder HiFi DNA Assembly Cloning Kit (New England Biolabs). In brief, the plasmid and *ppsD* insert were amplified by PCR and a Gibson assembly reaction was used to transform *Escherichia coli* DH5α. The plasmid was isolated, and the nucleotide sequence of the construct was verified by Sanger sequencing. H37Rv Δ*ppsD* cells were electroporated with ~0.5 μg of the complementation plasmid, recovered overnight in 7H9/OADC/glycerol/tyloxapol at 37 °C with shaking and then selected on plates containing hygromycin (75 μg/ml) and kanamycin (30 μg/ml). The H37Rv

559 Δ*ppsD*::comp strain was validated by PCR to confirm both the complementation and presence of
560 the Δ*ppsD* deletion. Primers used for vector construction and PCR confirmation are listed in
561 Supplementary Table 4.

562 **Thin layer chromatography**

563 *Mtb* cultures were grown to early log phase and then diluted to OD_{600} 0.3 in 10 ml
564 7H9/OADC/glycerol/tyloxapol and labelled with propionic acid [1-^{14}C] sodium salt (7 μCi)
565 (American Radiolabeled Chemicals, Inc.). Cultures were incubated with shaking at 37 °C for two
566 days and then spun down. Methanol (2.0 ml), 0.3% sodium chloride aqueous solution (0.2 ml) and
567 petroleum ether (2.0 ml) were added to the cell pellets and the suspensions were vortexed for 30 s
568 followed by centrifugation. The petroleum ether phases were moved to new tubes and the
569 extraction with petroleum ether was repeated twice. The petroleum phases were combined, dried
570 with anhydrous sodium sulfate, filtered and evaporated to dryness under nitrogen. The PDIM
571 extracts were resuspended in dichloromethane (0.2 ml). Counts per minute (cpm) were measured
572 to load approximately 5000 cpm for each sample on a silica gel 60 F254 thin layer chromatography
573 (TLC) plate (Sigma-Aldrich). The TLC plate was eluted three times with petroleum ether/ethyl
574 acetate 98/2. PDIMs were detected by autoradiograph after exposure for 48–72h at -80 °C. PDIM
575 band intensity was quantified using ImageJ (v 1.52a)[55].

576 **MIC assays**

577 Resistance of *Mtb* strains to vancomycin and other inhibitors (Supplementary Table 5)
578 were determined using the microbroth dilution method. Two-fold serial dilutions at 2 × final drug
579 concentration were prepared in standard 7H9/OADC/glycerol/tyloxapol or media supplemented
580 with either 2 × propionate (0.2 or 2.0 mM) or vitamin B_{12} (14.8 μM) at a volume of 100 μl in the
581 inner wells of flat-bottom 96-well plates. The outer wells were aliquoted with 200 μl PBS or

media. Strains were precultured in 7H9/OADC/glycerol/tyloxapol to OD_{600} of ~0.8 and then diluted to OD_{600} 0.01 in the same media. 100 µl of the cell dilution was added to plate to give a final OD_{600} of 0.005; 0.1 or 1.0 mM propionate or 7.4 µM vitamin B_{12} for supplemented assays; and 1 × drug concentration. Plates were incubated with gentle shaking and bacterial growth was measured by OD after 10 days unless otherwise specified. For BSL2 strains, OD_{600} was measured on a FLUOstar Omega Microplate Reader (BMG LABTECH). For BSL3 strains, OD_{590} was measured on an Epoch BioTek Microplate Spectrophotometer (BioTek Instruments, Inc.). Data were normalized to drug-free control wells and fit with non-linear regression in Prism (v9.4.1, v10.0.1) (GraphPad Software). MIC_{90} and MIC_{50} values were calculated from the curve fit.

VAN10 assay

VAN10 assays were performed in the inner wells of flat-bottom 96-well plates prepared with standard 7H9/OADC/glycerol/tyloxapol or media supplemented with 2 × propionate (0.2 or 2.0 mM) or vitamin B_{12} (14.8 µM). Triplicate wells were aliquoted with 100 µl drug-free media or media with 20 µg/ml vancomycin. Strains were precultured as for MIC assays and diluted to an OD_{600} of 0.01 in 7H9/OADC/glycerol/tyloxapol. 100 µl of the cell dilution was added to the plate giving a final vancomycin concentration of 10 µg/ml in treated wells (VAN10); OD_{600} of 0.005; and 0.1 or 1.0 mM propionate or 7.4 µM vitamin B_{12} in supplemented assays. Plates were incubated with gentle shaking and bacterial growth was measured by OD after 10 days unless otherwise specified. Relative growth in VAN10 was calculated compared to drug-free wells (VAN0) (VAN10 OD / VAN0 OD × 100 = VAN10 growth%). The VAN10 assay supplemented with 0.1 mM propionate is referred to as the 'VAN10-P' assay.

For high throughput screening of single colonies and to isolate PDIM(+) clones, single colonies were picked into 7H9/OADC/glycerol/tyloxapol and grown until dense to synchronize.

Outgrowth cultures were then subcultured for a single passage and grown to an OD_{600} of ~0.5–1.0. Subcultures were diluted 1:50 in 7H9/OADC/glycerol/tyloxapol and 100 µl of this was used to inoculate VAN10-P assay plates prepared as above. Growth was measured after 14 days to obtain an endpoint measurement. mc^26230 was additionally supplemented with 24 mg/l pantothenate, and 0.1 mM propionate was included in the plates and outgrowth media used to isolate mc^26230 AE1601 (Supplementary Table 1).

Permeability assay

Cell envelope permeability was determined using the Ethidium Bromide (EtBr) uptake assay[16]. Four replicate cultures of *Mtb* mc^27902 and mc^28398 in 10 ml 7H9/OADC/glycerol/ tyloxapol + PALM media were grown to an OD_{600} of 0.6–1.0. Cultures were washed three times with PBS + 0.4% (w/v) glucose and diluted to an OD_{600} of 0.5. Five replicate 180 µl aliquots were transferred to a black, clear-bottom, 96-well plate and 20 µl EtBr (50 µg/ml) was added. The plate was incubated at 37 °C in a FLUOstar Omega Microplate Reader (BMG LABTECH) with 300 rpm double-orbital shaking. Fluorescence was measured at an excitation wavelength of 355 nm and emission wavelength of 590 nm every 15 min for one hour.

Evolution experiments

Triplicate inkwells containing 10 ml standard 7H9/OADC/glycerol/tyloxapol or supplemented media as specified were inoculated with 100 µl of frozen *Mtb* seed stock and incubated for 7–10 days. Cultures were then diluted 1:250 into 10 ml fresh media each week for serial passage. To assess PDIM maintenance over the course of the experiment, at selected passages cultures were input into VAN10-P assays and 1 ml of culture was stocked and stored at -80 °C. VAN10-P assay plates were prepared as above and cultures were diluted 1:100 in 7H9/OADC/glycerol/tyloxapol for input into the assay. Growth was measured after 7 and 14 days

of incubation. For TLC lipid analysis of passaged cultures, cultures were first recovered from frozen stocks by growing to an OD_{600} of ~1.0 in standard 7H9/OADC/glycerol/tyloxapol before ^{14}C-labelling and TLC lipid analysis as above.

Metabolomics extractions

Triplicate inkwells containing 7 ml standard 7H9/OADC/glycerol/tyloxapol or supplemented media as specified were inoculated at OD_{600} 0.01 and grown for five days and then harvested. An equivalent of 3 ml culture at an OD_{600} of 1.0 was rapidly filtered on 0.45 µm Durapore PVDF membrane filters (MilliporeSigma) using a vacuum manifold (MilliporeSigma). Cultures were quenched by placing the filter paper in 1 ml of extraction solvent containing 20:40:40 (v/v) water/acetonitrile/methanol with approximately 500 µl of 0.1 mm zirconia/silica beads (BioSpec) at -20 °C. Samples were homogenized using a Precellys Cryolys Evolution (Bertin Technologies) cooled to 0 °C for three 20 s cycles at 6800 rpm with a 30 s pause between cycles. Samples were centrifuged and the extracts were filtered through a 0.22 µm Nylon Spin-X microcentrifuge filter (Corning) and stored at -80 °C. For analysis, extract samples were concentrated 5-fold by using a SpeedVac® Plus SC110A (Savant Instruments, Inc.) to evaporate the solvent and then redissolved in 1/5th volume of the extraction solvent.

LC-MS metabolomic profiling

Metabolomics analysis was performed using an Agilent 1290 Infinity II liquid chromatography (LC) system coupled with an Agilent 6545 quadrupole time-of-flight (QTOF) mass spectrometer (MS) equipped with a Dual Agilent Jet Stream Electrospray Ionization (Dual AJS ESI) source operated in negative mode. Metabolites were separated on an InfinityLab Poroshell 120 HILIC-Z, 2.1 x 150 mm, 2.7 µm, 100 Å column (Agilent) based on previously described methods[56]. The mobile phase consisted of solvent A: water, and solvent B: 15:85 (v/v)

651 water/acetonitrile, both with 10 mM ammonium acetate and 2.5 µM InfinityLab Deactivator
652 Additive (Agilent), pH 9.0. HPLC grade water (Cen-Med Enterprises) and LC-MS grade solvents
653 (Fisher Chemical) were used for both the LC-MS mobile phase and metabolite extraction. The
654 elution gradient used was as follows: 0–2 min 96% B; 2–5.5 min 96 to 88% B; 5.5–8.5 88% B;
655 8.5–9 min 88 to 86% B; 9–14 min 86% B; 14–17 min 86 to 82% B; 17–23 min 82 to 65% B; 23–
656 24 min 65% B; 24–24.5 min 64 to 96% B; 24.5–26 min 96% B; followed by a 3 min re-
657 equilibration at 96% B. The flow rate was 0.25 ml/min and column temperature 50 °C. The
658 injection volume was 3 µl and the autosampler was maintained at 4 °C during the run. Mass spectra
659 were recorded in profile mode from *m/z* 60 to 1200 using an acquisition rate of 1 spectra/s in the
660 2GHz extended dynamic range mode and 1700 m/z low mass range, using the sensitive slicer mode
661 and fragile ions option. The gas temperature was 225 °C and sheath gas temperature 350 °C. The
662 capillary, nozzle, fragmentor, skimmer, and octopole voltages were 3500, 2000, 125, 45 and
663 750 V, respectively. Dynamic mass axis calibration was achieved by continuous infusion of a
664 reference mass solution using an isocratic pump with a 100:1 splitter.

665 Data Analysis was performed using the Agilent MassHunter Qualitative and Quantitative
666 Analysis Software. Metabolite identification was based on mass-retention times determined using
667 chemical standards (Supplementary Table 6) and isotope distribution patterns. Calibration curves
668 of standard compound mixtures in extraction buffer and spiked into a homologous mycobacterial
669 extract were run to determine the linear range. Metabolites were quantified using a mass tolerance
670 of 20 ppm with manual curation of peak areas where necessary and the area under the curve (AUC)
671 was determined. AUC was normalized using the median total AUC for a panel of 50 putative
672 metabolites across different metabolic pathways (Supplementary Table 7) to correct for differences
673 in extraction and concentration efficiency.

Mouse experiments

Mouse experiments were performed in accordance with National Institutes of Health guidelines following the recommendations in the Guide for the Care and Use of Laboratory Animals[57]. The protocols used in this study were approved by the Institutional Animal Care and Use Committee of Albert Einstein College of Medicine (Protocols #00001445 and #00001332). To generate H37Rv-B, female C57BL/6 mice (Jackson Laboratory) were infected with H37Rv-A via the aerosol route using a 1×10^7 cfu/ml *Mtb* suspension in PBS containing 0.05% tyloxapol and 0.004% antifoam. Mice were sacrificed after 21 days and the lungs homogenized and plated on 7H10/OADC/glycerol plates. All colonies from the lung of a single mouse were harvested and used to inoculate 7H9/OADC/glycerol/tyloxapol in a roller bottle. This was grown to an OD_{600} of 1.8 and then stocked in 1 ml aliquots and stored at -80 ºC. To isolate single PDIM(+) clones of Erdman, HN878 and CDC1551, in-house bred $Rag^{-/-}$ mice were infected with 5×10^6 cfu/mouse via the intravenous route. Mice were killed on day 20 post-infection and the lungs homogenized and plated on 7H10/OADC/glycerol plates. Single colonies were picked and outgrown in 7H9/OADC/glycerol/tyloxapol with 0.1 mM propionate for stocking and then subcultured and screened for PDIM using VAN10-P assays as above.

Whole genome sequencing and analysis

Genomic DNA was isolated using a CTAB extraction method as previously described[58] and sequenced in-house on an Illumina MiSeq. Genomic libraries were prepared using the Illumina Nextera XT library preparation kit and sequenced with a 600-cycle v3 reagent kit (2×301 bp reads) following the manufacturer's instructions. Genomes with uneven coverage (< 90% of the genome having > 10 × coverage) for which no PDIM SNPs were detected were additionally sequenced with a 150-cycle v3 kit (2×76 bp reads) and the data merged for mapping. Additional

sequencing by Illumina NextSeq was performed by SeqCenter (Pittsburgh, PA) using the Illumina DNA Prep kit and sequenced on an Illumina NextSeq 2000 (2 × 151 bp reads).

Raw reads were trimmed with Trimmomatic (v0.39)[59] using a sliding window quality filter (SLIDINGWINDOW:4:15) and reads less than 25 bp were discarded (MINLEN:25). Trimmed reads were then mapped to the reference genome corresponding to the strain background (H37Rv NC_000962.3, CDC1551 NC_002755.2, Erdman NC_020559.1, HN878 NZ_CM001043.1 and KZN 4207 NC_016768.1) using BWA-MEM (v0.7.17-r1188) (https://github.com/lh3/bwa). Mapping files were sorted and indexed using Samtools (v1.6)[60]. Duplicates were removed using Picard tools (v2.26.10) (http://broadinstitute.github.io/picard) and local realignment was performed using GATK (v.3.8-0)[61]. Mapping quality was assessed using Qualimap (v2.2.1)[62]. Variants were called using Pilon (v1.23)[63] using a minimum depth threshold of 5, base quality threshold of 15 and mapping quality threshold of 40 (--variant --mindepth 5 --minqual 15 --minmq 40). Variants were annotated using SNPeff (v5.1d)[64]. Geneious Prime® (v2022.2.2) (Biomatters Ltd.) was used to detect low-frequency variants within the PDIM gene region (*tesA–Rv2953*) using the variation/SNP finder feature with a coverage threshold of 10, minimum variant frequency of 10%, and P value $< 1 \times 10^{-10}$. SeqTK (v1.3-r106) (https://github.com/lh3/seqtk) was used to randomly subsample reads for downsampling analyses.

***ppsC* homopolymeric tract region Sanger sequencing**

To identify and confirm mutations in the *ppsC* homopolymeric tract region, a 250 bp fragment encompassing this region was amplified by PCR and then sequenced by Sanger sequencing. PCR was performed in 50 µl reactions containing 2.5 units HOT FIREPol® DNA polymerase (Solis BioDyne), the supplied reaction buffer BD at 1 × concentration, 2.0 mM $MgCl_2$, 250 µM dNTPs, 0.3 µM of each primer, and 2.5% (v/v) DMSO. Primers are listed in

Supplementary Table 4. Approximately 25 ng of gDNA was used as the PCR template. Thermal cycling consisted of an initial denaturation and enzyme activation step of 15 min at 95 °C, followed by 35 cycles of 30 s at 95 °C, 45 s at 55 °C, and 30 s at 72 °C. This was followed by a final elongation step of 10 min at 72 °C. PCR products were purified using the Wizard® SV Gel and PCR Clean-Up system (Promega) and then sequenced by Sanger sequencing at GENEWIZ (South Plainfield, NJ) in both the forward and reverse direction using the same primers as for amplification.

Statistical analysis

Statistical analyses were performed using Prism (v9.4.1 and v10.0.) (GraphPad Software). Significant differences were calculated by one- or two-way ANOVA using multiple comparison tests as specified, or the nonparametric Mann-Whitney test for skewed data. Correlations between vancomycin MIC and VAN10 growth% with PDIM were assessed by simple linear regression.

Data availability

Whole genome sequence data have been deposited in the NCBI Sequence Read Archive (SRA) under the BioProject accession number PRJNA923717. A complete list of strains sequenced in this study and SRA accession numbers are given in Supplementary Table 8. Raw metabolomics data are provided as a source data file.

Methods References

54 Stover, C. K. *et al.* New use of BCG for recombinant vaccines. *Nature* **351**, 456-460 (1991). https://doi.org:10.1038/351456a0

55 Schneider, C. A., Rasband, W. S. & Eliceiri, K. W. NIH Image to ImageJ: 25 years of image analysis. *Nat Methods* **9**, 671-675 (2012). https://doi.org:10.1038/nmeth.2089

56 Dai, Y. & Hsiao, J. J. Discovery Metabolomics LC/MS Methods Optimized for Polar Metabolites. *Application note, Agilent Technologies, Inc.* (2019).

57 National Research Council of the National Academies. *Guide for the Care and Use of Laboratory Animals: Eighth Edition*. (National Academies Press, 2011).

58 Wilson, K. Preparation of genomic DNA from bacteria. *Curr Protoc Mol Biol* **56**, 2.4.1-2.4.5 (2001). https://doi.org:10.1002/0471142727.mb0204s56

59 Bolger, A. M., Lohse, M. & Usadel, B. Trimmomatic: a flexible trimmer for Illumina sequence data. *Bioinformatics* **30**, 2114-2120 (2014). https://doi.org:10.1093/bioinformatics/btu170

60 Danecek, P. *et al.* Twelve years of SAMtools and BCFtools. *Gigascience* **10** (2021). https://doi.org:10.1093/gigascience/giab008

61 DePristo, M. A. *et al.* A framework for variation discovery and genotyping using next-generation DNA sequencing data. *Nat Genet* **43**, 491-498 (2011). https://doi.org:10.1038/ng.806

62 Okonechnikov, K., Conesa, A. & Garcia-Alcalde, F. Qualimap 2: advanced multi-sample quality control for high-throughput sequencing data. *Bioinformatics* **32**, 292-294 (2016). https://doi.org:10.1093/bioinformatics/btv566

759 63 Walker, B. J. *et al.* Pilon: an integrated tool for comprehensive microbial variant detection
760 and genome assembly improvement. *PLoS One* **9**, e112963 (2014).
761 https://doi.org:10.1371/journal.pone.0112963
762 64 Cingolani, P. *et al.* A program for annotating and predicting the effects of single nucleotide
763 polymorphisms, SnpEff: SNPs in the genome of Drosophila melanogaster strain w1118;
764 iso-2; iso-3. *Fly (Austin)* **6**, 80-92 (2012). https://doi.org:10.4161/fly.19695
765 65 Sambandamurthy, V. K. *et al.* Mycobacterium tuberculosis DeltaRD1 DeltapanCD: a safe
766 and limited replicating mutant strain that protects immunocompetent and
767 immunocompromised mice against experimental tuberculosis. *Vaccine* **24**, 6309-6320
768 (2006). https://doi.org:10.1016/j.vaccine.2006.05.097
769 66 Jain, P. *et al.* phi(2)GFP10, a high-intensity fluorophage, enables detection and rapid drug
770 susceptibility testing of Mycobacterium tuberculosis directly from sputum samples. *J Clin*
771 *Microbiol* **50**, 1362-1369 (2012). https://doi.org:10.1128/JCM.06192-11
772 67 Vilcheze, C. *et al.* Rational Design of Biosafety Level 2-Approved, Multidrug-Resistant
773 Strains of Mycobacterium tuberculosis through Nutrient Auxotrophy. *mBio* **9** (2018).
774 https://doi.org:10.1128/mBio.00938-18

Acknowledgments

We thank Bing Chen, John Kim, and Mei Chen for assistance with animal experiments; Annie Zhi Dai for technical support; and the labs of Jeremy Rock, Rockefeller University, NY, and John Chan, Rutgers University, NJ, for their feedback and independent validation of VAN-P PDIM assays. C.V.M., T.J.W., J.C., E.Z.R., and M.B. acknowledge support from the National Institutes of Health/National Institute of Allergy and Infectious Diseases (R01 AI139465 and R01 AI175972), the Potts Memorial Foundation, and Albert Einstein College of Medicine internal funding. M.W.S. acknowledges support from the Institutional AIDS training grant, Training in HIV/AIDS Pathogenesis; Basic and Translational Research (T32 AI007501), and the Albert Einstein College of Medicine MSTP training grant.

Author contributions

C.V.M. and M.B. conceived and designed the study. C.V.M., T.J.W., J.C., C.V., S.R., M.W.S., and E.Z.R., performed the experiments. C.V.M., T.J.W., C.V., M.W.S., and M.B. analysed the data. M.B. and W.J.R. provided resources. C.V.M. and M.B. wrote the paper. T.J.W., C.V., S.R., M.W.S., E.Z.R., and W.J.R. critically reviewed and edited the paper.

Competing interests

C.V.M. and M.B. are inventors on a pending patent related to this work (US Patent Application No. 63/527,831, filed 20 July 2023). The authors declare that they have no other competing interests.

Additional information

Supplementary Information is available for this paper.

Correspondence and requests for materials should be addressed to M.B.

Reprints and permissions information is available at www.nature.com/reprints

Strain	Genome coverage (×)			PDIM mutations
	Mean	SD	≥ 10 ×	
mc²6206	66.3	17.4	99.00%	n.d.
mc²6209	56.8	21.8	98.90%	n.d.
mc²6230	187.0	73.8	98.50%	*ppsC* c.2685(C)$_{7\to8}$ (66%)†
mc²6230 AE1601*	171.7	32.6	99.11%	n.d.
mc²6230 AE1611	30.5	9.4	97.26%	*ppsC* c.2685(C)$_{7\to8}$ ‡
mc²7901	26.7	10.5	96.50%	*fadD28* p.Arg562Gly
mc²7902	47.8	15.9	98.50%	n.d.
mc²8398	62.1	16.7	99.20%	*ppsC* c.2475delC
H37Rv-A	93.5	31.0	97.60%	n.d.
H37Rv-B	60.5	18.3	97.80%	n.d.
H37Rv-SC (AE1028)*	57.1	19.6	98.90%	n.d.
H37Rv Δ*ppsD*	58.7	18.6	98.70%	Δ*ppsD*
H37Rv Δ*tgs1*-1	95.6	56.5	91.70%	*fadD28* p.Leu241Pro
H37Rv Δ*tgs1*-2	90.3	78.6	83.00%	*ppsA* p.Trp968*
H37Rv Δ*tgs1*-3	17.2	7.0	87.20%	*ppsD* p.Ser247Pro
H37Rv Δ*tgs1*-4	86.3	25.1	97.70%	*ppsE* p.Asp74Asn
H37Rv Δ*tgs1*-5	119.4	57.2	96.50%	*ppsC* c.2668(C)$_{7\to6}$ ‡
H37Rv Δ*tgs1*-7	184.5	138.4	93.10%	n.d.
H37Rv Δ*tgs1*-8	58.2	15.1	99.00%	*ppsC* c.2668(C)$_{7\to8}$ ‡
H37Rv Δ*tgs1*-9	69.7	18.0	99.10%	*ppsC* c.2668(C)$_{7\to6}$ ‡
CDC1551-A	106.5	49.8	96.90%	n.d.
CDC1551-B	54.7	19.6	98.80%	n.d.
CDC1551 Δ*mas*	44.0	18.6	96.50%	Δ*mas*
Erdman	84.7	25.2	98.00%	*ppsA* c.3418insA (72%)
HN878	76.1	44.3	93.10%	n.d.
KZN 4207	86.7	38.1	97.10%	n.d.
CDC1551-SC (AE5005)*	69.3	18.9	99.10%	n.d.
Erdman-SC (AE3003)*	91.2	23.5	99.30%	n.d.
HN878-SC (AE8005)*	65.9	24.4	97.90%	n.d.
H37Rv-B col5 (VAN10-P 41%)	61.0	15.7	99.00%	*ppsE* p.Asp74Asn
H37Rv-B col6 (VAN10-P 1%)	53.9	14.8	98.70%	*ppsA* p.Trp968*
H37Rv-B col16 (VAN10-P 43%)	50.7	13.7	98.60%	*ppsE* p.Asp74Asn
H37Rv-B col17 (VAN10-P 77%)	34.9	13.0	97.90%	n.d.
H37Rv-B col19 (VAN10-P 31%)	94.0	25.0	99.10%	*ppsE* p.Asp74Asn
H37Rv-B col23 (VAN10-P 39%)	38.2	11.2	98.10%	*ppsE* p.Asp74Asn
H37Rv-B col36 (VAN10-P 1%)	62.9	15.7	98.90%	*ppsA* p.Trp968*

*PDIM(+) clone identified by VAN10-P screening of single colonies (see also Extended data Fig. 4). †Mutation identified using the Illumina NextSeq platform; ‡Mutation detected/confirmed by PCR and Sanger sequencing (see also Extended data Fig. 5). n.d. = no non-synonymous PDIM mutations detected.

Extended Data Table 1 | PDIM mutations in *Mtb* strains included in this study. Non-synonymous variants in genes involved in PDIM biosynthesis, assembly, processing, or transport (see Fig. 2e). Mutations are described at the protein level for amino acid substitutions (p.) and at the gene coding level for frameshift/INDEL mutations (c.). Variants were identified from Illumina MiSeq WGS data using the software tool Pilon[63] for variant calling unless indicated. For mutations with mixed coverage (< 90%) the frequency of the variant allele is given in brackets. 'H37Rv-B col#' are single colonies isolated from H37Rv-B with different VAN10-P growth%, including a

809 subset of those which had an intermediate VAN10-P phenotype (see Fig. 2f). '≥ 10 ×' is the

810 percentage of genome with 10 × or greater coverage.

Strain	PDIM mutations	Frequency	REF/ALT	*P* value
H37Rv-A	*ppsB* p.Leu250Pro	11.6%	99/13	3.1×10^{-23}
H37Rv-B	n.d.			
Erdman	*ppsA* c.3418insA	67.9%	27/57	2.9×10^{-161}
	ppsE p.Cys414*	10.7%	50/6	3.2×10^{-14}
KZN 4207	n.d.			
HN878	*fadD28* c.347delT	14.3%	126/21	2.6×10^{-30}
	ppsD p.Gly1636Arg	18.8%	26/6	1.4×10^{-14}
CDC1551-A	*ppsA* p.Phe327Val	10.2%	115/13	7.1×10^{-20}
	ppsE c.3496insA	12.6%	118/17	9.9×10^{-41}
CDC1551-B	n.d.			

Extended Data Table 2 | Low-frequency PDIM mutation analysis. Low-frequency non-synonymous PDIM variants detected in laboratory stocks of virulent *Mtb* strains (Fig. 2a). Variant calling was performed using the Geneious variant finder with the following thresholds: ≥ 10% variant frequency, ≥ 10 × coverage, $P < 1 \times 10^{-10}$. n.d. = none detected.

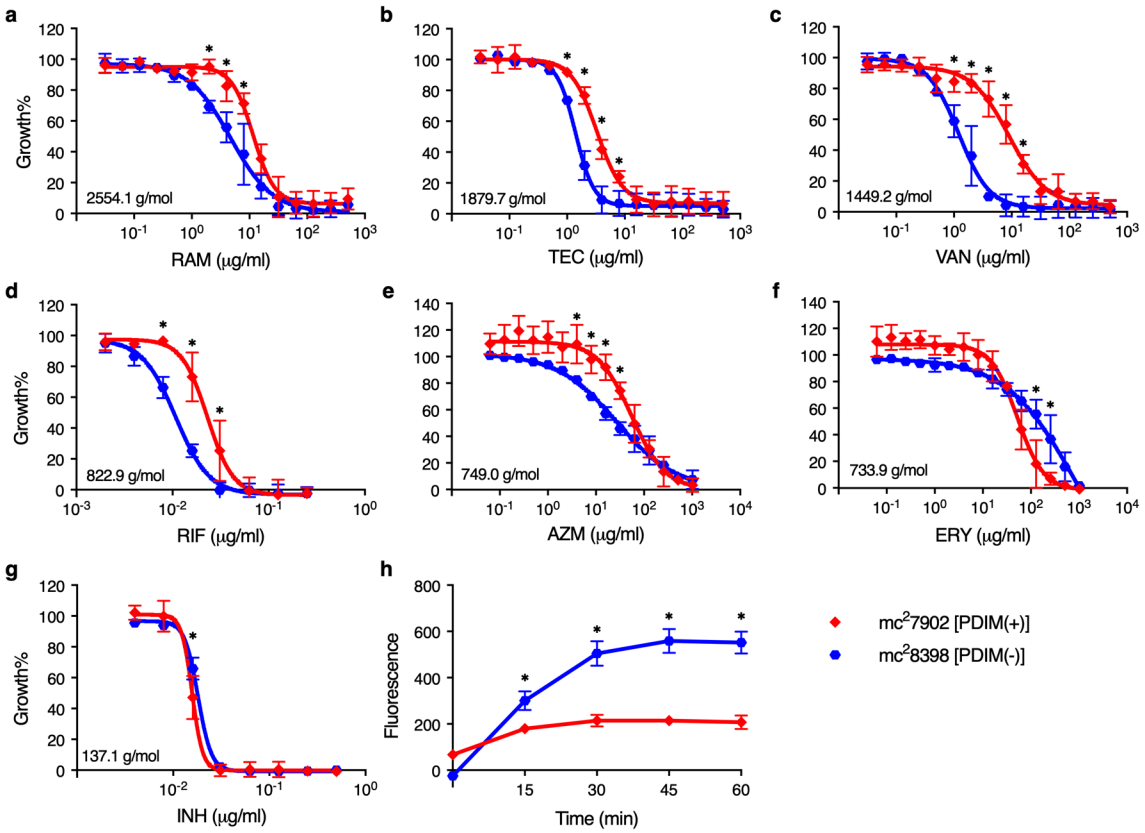

816

817 **Extended Data Fig. 1 | Resistance of PDIM(-) and PDIM(+) *Mtb* to high molecular weight**
818 **compounds. a**–**g**, MIC assays of *Mtb* mc²7902 [PDIM(+)] and mc²8398 [PDIM(-)] to (**a**)
819 ramoplanin (RAM), (**b**) teicoplanin (TEC), (**c**) vancomycin (VAN), (**d**) rifampicin (RIF), (**e**)
820 azithromycin (AZM), (**f**) erythromycin (ERY), and (**g**) isoniazid (INH). Compounds are arranged
821 by descending molecular weight, which is shown on the MIC plots. MICs were performed in
822 7H9/OADC/glycerol/tyloxapol + PALM media and bacterial growth was measured after 10 days
823 of incubation and normalized to drug-free controls. Mean ± SD for $n = 4$ biological replicates from
824 two independent experiments. **h**, Ethidium Bromide uptake of mc²7902 and mc²8398. Uptake in
825 whole cell suspensions was monitored by fluorescence (Ex 355 nm/Em 590 nm). Mean ± SD for
826 $n = 4$ biological replicates, each measured in five technical replicates. Uptake data are

827 representative of two independent experiments. *$P < 0.001$; two-way ANOVA with Šidák's

828 multiple comparison test.

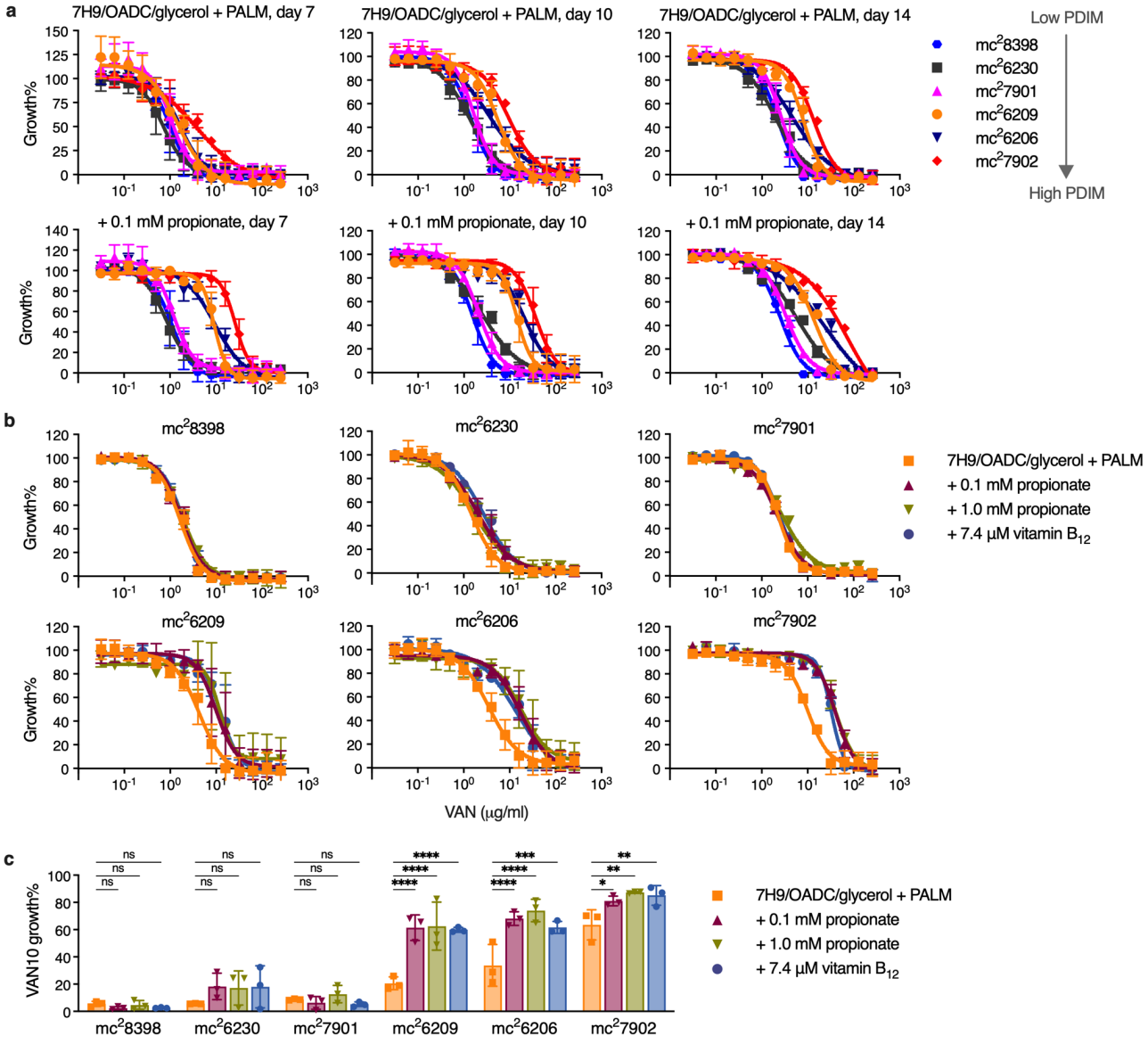

829

830 **Extended Data Fig. 2 | Propionate and vitamin B_{12} supplementation selectively increase**
831 **vancomycin resistance of PDIM(+) *Mtb* improving assay robustness and reducing time to**
832 **result. a**, Vancomycin MICs for the PDIM reference strain set in standard
833 7H9/OADC/glycerol/tyloxapol + PALM media and additionally supplemented with 0.1 mM
834 propionate. Growth was measured after 7, 10, and 14 days as indicated. **b**, Vancomycin MICs in
835 standard media and additionally supplemented with 0.1 or 1.0 mM propionate or 7.4 µM

vitamin B_{12}. Growth was measured after 10 days. Mean ± SD for $n = 4$ biological replicates from two independent experiments. **c**, VAN10 assays in standard and supplemented media. Growth was measured after 10 days. Mean ± SD for $n = 3$ independent experiments, each performed in triplicate. *$P < 0.05$, **$P < 0.01$, ***$P < 0.001$, ****$P < 0.0001$; two-way ANOVA with Šidák's multiple comparison test. The day seven data in (**a**) are additionally shown in Fig. 1c and are shown here alongside additional time points. The data in (**b**) includes one of the same experiments shown in (**a**), together with data from an independent experiment. The VAN10-P (+ 0.1 mM propionate) data in (**c**) are additionally shown in Fig. 1e and are shown here alongside additional conditions.

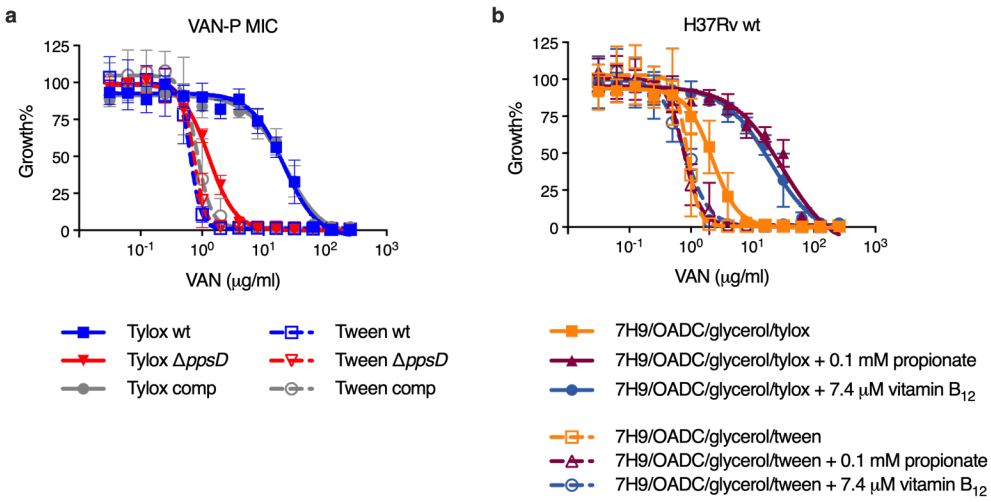

844

845 **Extended Data Fig. 3 | Tween 80 decreases vancomycin resistance and abolishes PDIM-**
846 **related differences in MIC. a**, VAN-P MICs for isogenic PDIM(+) and PDIM(-) *Mtb* H37Rv
847 using either tyloxapol or Tween 80 as the culture detergent. **b**, Vancomycin MICs for PDIM(+)
848 H37Rv wildtype in standard 7H9/OADC/glycerol media and supplemented with propionate or
849 vitamin B_{12} using either tyloxapol or Tween 80 as the detergent. Mean ± SD for $n = 4$ biological
850 replicates from two independent experiments.

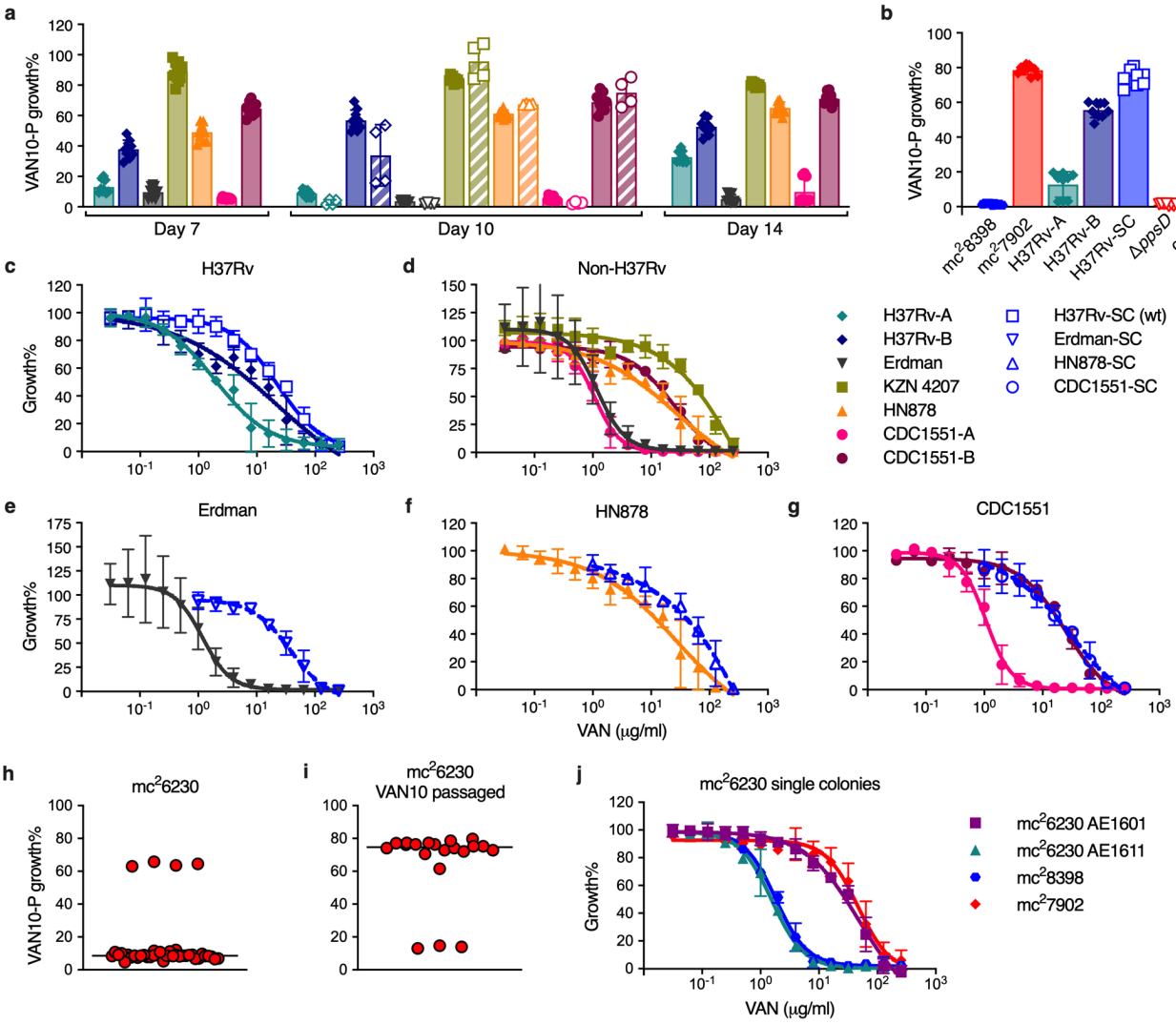

851

852 **Extended Data Fig. 4 | VAN-P assays predict PDIM levels across different *Mtb* strains and**
853 **lineages and enable re-isolation of single PDIM(+) clones. a**, VAN10-P assays for a range of
854 virulent *Mtb* strains belonging to different lineages. Bacterial growth was measured after 7, 10,
855 and 14 days of incubation as indicated. Data are from the same experiment in Fig. 2a and show
856 additional time points plus an independent experimental repeat measured on day 10 (hatched bars
857 with unfilled symbols). **b**, VAN10-P assays for strains with an H37Rv background including
858 mc²7902 and mc²8398. H37Rv-SC is a single PDIM(+) clone isolated from H37Rv-B by

VAN10-P colony screening. This clone was used as our PDIM(+) H37Rv wildtype strain throughout this work and was used to construct H37Rv Δ*ppsD* and Δ*ppsD*::comp isogenic mutants (Supplementary Table 2). Data in (**a**,**b**) show mean ± SD for $n = 9$ pairwise comparisons between triplicate wells, except for the day 10 repeat in (**a**) where $n = 4$ pairwise comparisons between duplicate wells. **c**, VAN-P MICs of H37Rv stocks and H37Rv-SC. **d**, VAN-P MICs of non-H37Rv strains from (**a**). **e**–**g**, VAN-P MICs of single PDIM(+) clones isolated from $Rag^{-/-}$ mice using VAN10-P colony screening for (**e**) Erdman, (**f**) HN878, and (**g**) CDC1551 (see also Extended Data Table 1). Data are plotted together with MIC data from (**d**) for comparison. MIC data in (**c**–**g**) show mean ± SD for $n = 4$ biological replicates from two independent experiments. **h**–**j**, Determination that our *Mtb* $mc^2$6230 stock is a mixed population and re-isolation of a single PDIM(+) clone by VAN10-P screening. (**h**) VAN10-P assay of single colonies isolated from our $mc^2$6230 stock ($n = 40$) and (**i**) following a single passage in 10 μg/ml vancomycin ($n = 20$). Vancomycin significantly enriched for PDIM(+) bacilli ($P < 0.0001$ two-tailed Mann-Whitney test), facilitating re-isolation of low-frequency PDIM(+) clones. Each colony was assayed in triplicate and data points represent mean VAN10-P growth%. Lines indicate the median. **j**, VAN-P MICs of PDIM(+) (AE1601) and PDIM(-) (AE1611) $mc^2$6230 clones identified by VAN10-P colony screening (see also Extended Data Table 1). Mean ± SD for $n = 6$ biological replicates from two independent experiments.

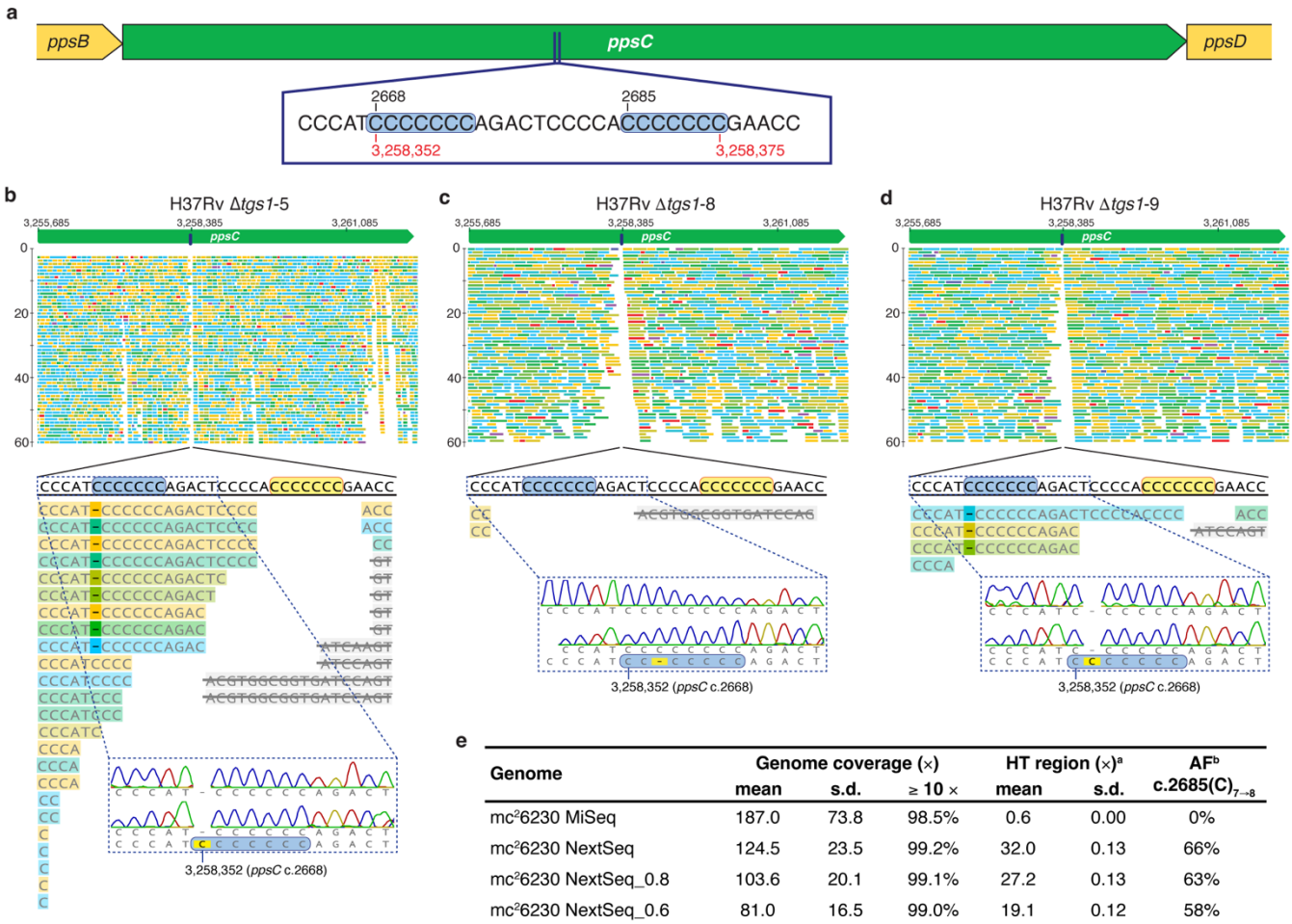

e

Genome	Genome coverage (×)			HT region (×)[a]		AF[b]
	mean	s.d.	≥ 10 ×	mean	s.d.	c.2685(C)$_{7\to8}$
mc²6230 MiSeq	187.0	73.8	98.5%	0.6	0.00	0%
mc²6230 NextSeq	124.5	23.5	99.2%	32.0	0.13	66%
mc²6230 NextSeq_0.8	103.6	20.1	99.1%	27.2	0.13	63%
mc²6230 NextSeq_0.6	81.0	16.5	99.0%	19.1	0.12	58%
mc²6230 NextSeq_0.4	56.4	12.4	98.8%	19.6	0.14	68%
mc²6230 NextSeq_0.2	29.6	7.7	98.2%	5.5	0.16	80%

[a] Read depth over the *ppsC* homopolymeric tract region (3258352-3258375)

[b] Allele frequency of the *ppsC* c.2685(C)$_{7\to8}$ frameshift mutation.

Extended Data Fig. 5 | Assessment of *ppsC* homopolymeric tract mutations. a, Schematic showing the location of a homopolymeric tract region in the *ppsC* gene. Sequence inserts show two adjacent 7-cytosine homopolymeric tracts (c.2668 and c.2685) ± 5 bp on either side. Numbers in black indicate the position in the *ppsC* gene and numbers in red the genomic position in the H37Rv genome. **b**–**d**, Analysis of the *ppsC* homopolymeric tract region in Δ*tgs1* mutants and identification of frameshift variants. WGS variant calling failed to identify PDIM mutations in Δ*tgs1*-5, Δ*tgs1*-8 and Δ*tgs1*-9 despite a PDIM(-) result in VAN-P MICs (Fig. 2b) and validation

of Δ*tgs1*-9 as PDIM(-) by TLC (Fig. 2c). Close manual inspection of WGS reads showed the *ppsC* homopolymeric tract region is poorly covered by Illumina MiSeq and identified potentially missed variant calls. PCR and Sanger sequencing confirmed the presence of a 2668$(C)_{7\rightarrow6}$ frameshift mutation in both Δ*tgs1*-5 (**b**) and Δ*tgs1*-9 (**d**) and identified a 2668$(C)_{7\rightarrow8}$ mutation in Δ*tgs1*-8 that was not covered at all by WGS (**c**). (**b**–**d**) were created with Geneious Prime® 2022.2.2 and Illustrator 26.4.1. Coverage has been cropped to a read depth of 60 ×. **e**, Identification of an unfixed *ppsC* c.2685$(C)_{7\rightarrow8}$ frameshift mutation in mc^26230 by Illumina NextSeq. VAN-P assays and TLC lipid analysis determined mc^26230 is highly PDIM deficient (Fig. 1a,c,e), however, WGS initially failed to identify any PDIM mutations in this strain and we subsequently established our mc^26230 stock is a mixed population (Extended Data Fig. 4h). Resequencing using the Illumina NextSeq platform identified an unfixed frameshift mutation in *ppsC* (c.2685$(C)_{7\rightarrow8}$) that was not detected by Illumina MiSeq due to poor coverage. To assess the relationship between overall coverage and coverage over the homopolymeric region NextSeq reads were randomly downsampled. The number following 'NextSeq_' represents the fraction of reads sampled (i.e. 0.8 = 80% of reads retained).

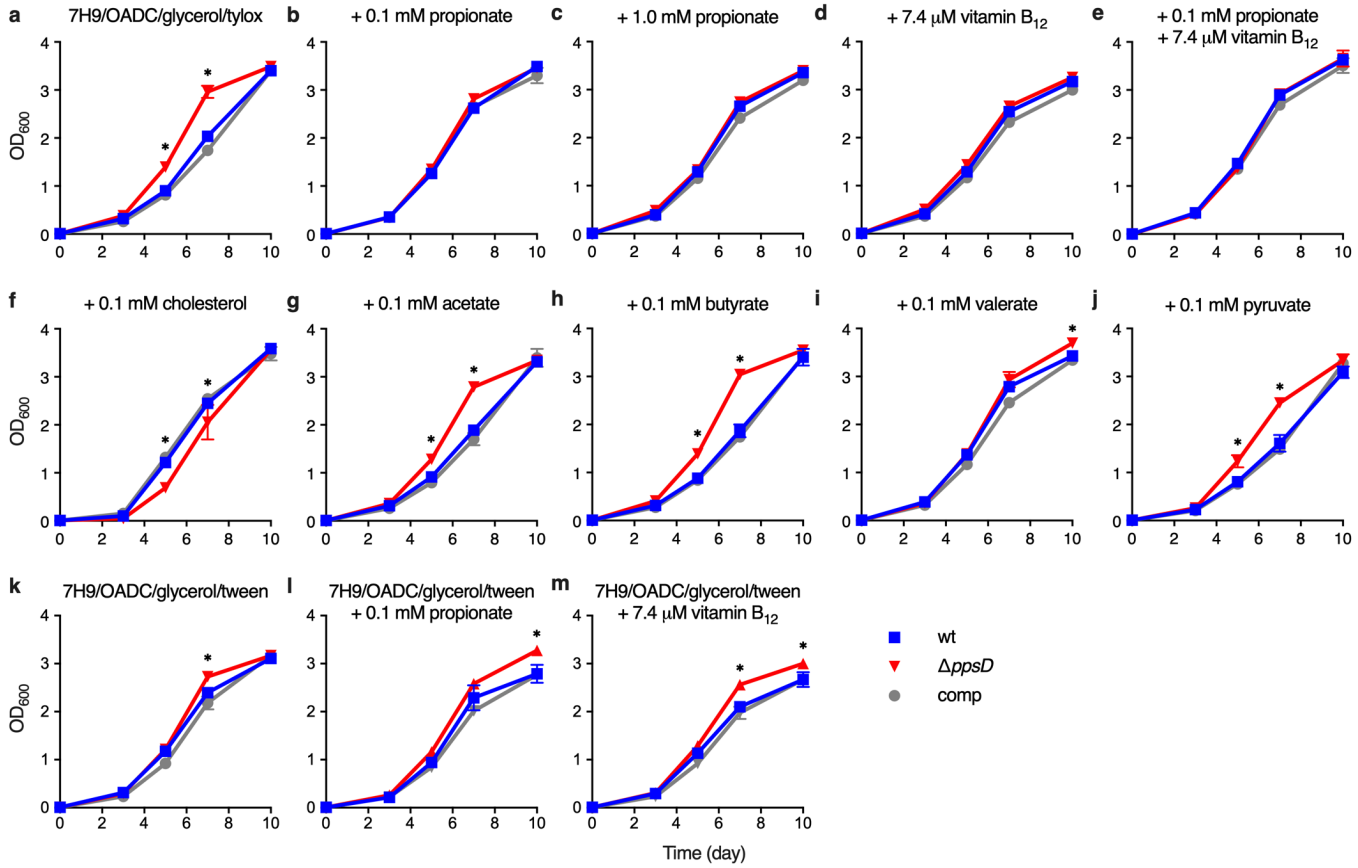

900

901 **Extended Data Fig. 6 | Effect of different media supplements on growth of PDIM(+) and**
902 **PDIM(-) *Mtb*.** **a**, Growth of PDIM(+) and PDIM(-) *Mtb* H37Rv in standard
903 7H9/OADC/glycerol/tyloxapol and **b**–**j**, the same media with additional supplements as indicated.
904 **k**–**m**, Growth using Tween 80 instead of tyloxapol as the culture detergent. (**k**)
905 7H9/OADC/glycerol/Tween 80 and (**l**) the same media supplemented with 0.1 mM propionate, or
906 (**m**) 7.4 μM vitamin B_{12}. Mean ± SD for $n = 3$ biological replicates. Data are representative of at
907 least two independent experiments. (**a**,**b**,**d**,**f**) show independent experimental repeats for the
908 conditions in Fig. 3b–e. *$P < 0.001$ for both wt and comp versus Δ*ppsD*; two-way ANOVA with
909 Tukey's multiple comparison test. For some data points the SD is smaller than the data symbols.

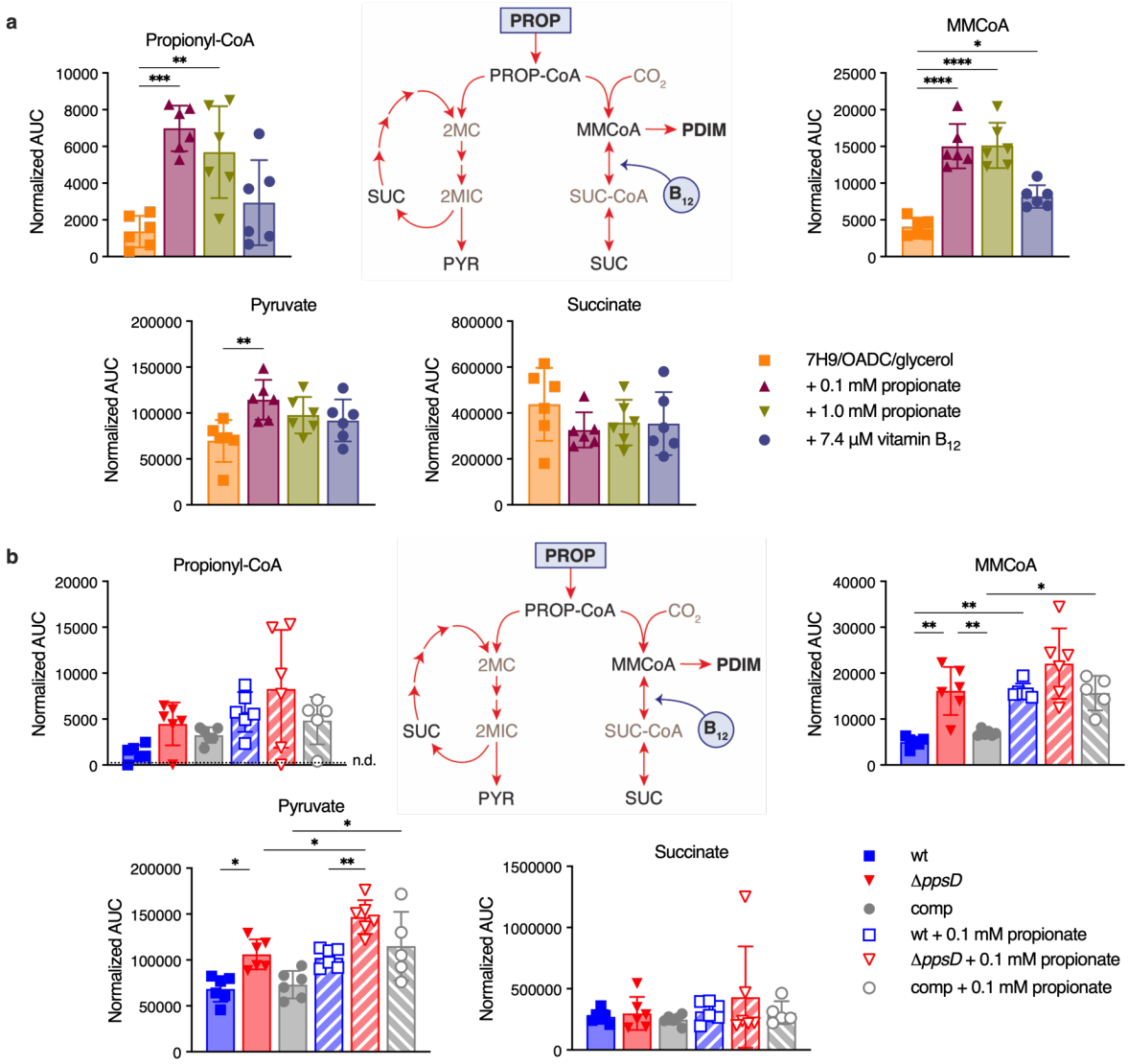

910

911 **Extended Data Fig. 7 | Effects of propionate and vitamin B_{12} supplementation on MMCoA**
912 **and propionyl-CoA metabolic pathways in *Mtb*.** **a**, Abundance of metabolites in propionyl-CoA
913 and MMCoA metabolism in PDIM(+) *Mtb* H37Rv wildtype grown in standard
914 7H9/OADC/glycerol/tyloxapol media and supplemented with propionate or vitamin B_{12}, and **b**, in
915 PDIM(+) and PDIM(-) H37Rv grown in 7H9/OADC/glycerol/tyloxapol ± 0.1 mM propionate.
916 Abundances are shown as normalized area under the curve (AUC). Mean ± SD for $n = 6$ biological
917 replicates from two independent experiments. $^{*}P < 0.05$, $^{**}P < 0.01$, $^{***}P < 0.001$,

****$P < 0.0001$; one-way ANOVA with Tukey's multiple comparison test. Significant differences compared to unsupplemented media are indicated in (**a**), and between ± propionate for each strain and between strains for each condition in (**b**). PROP, propionate; PROP-CoA, propionyl-CoA; MMCoA, methylmalonyl-CoA; SUC-CoA, succinyl-CoA; SUC, succinate; 2MC/2MIC, 2-methyl(iso)citrate; and PYR, pyruvate. Succinyl-CoA and methyl(iso)citrate were not able to be detected by our method. Propionyl-CoA was close to the detection limit and was not detected in all samples (n.d. = not detected). The data for MMCoA are also shown in Fig. 3f,g.

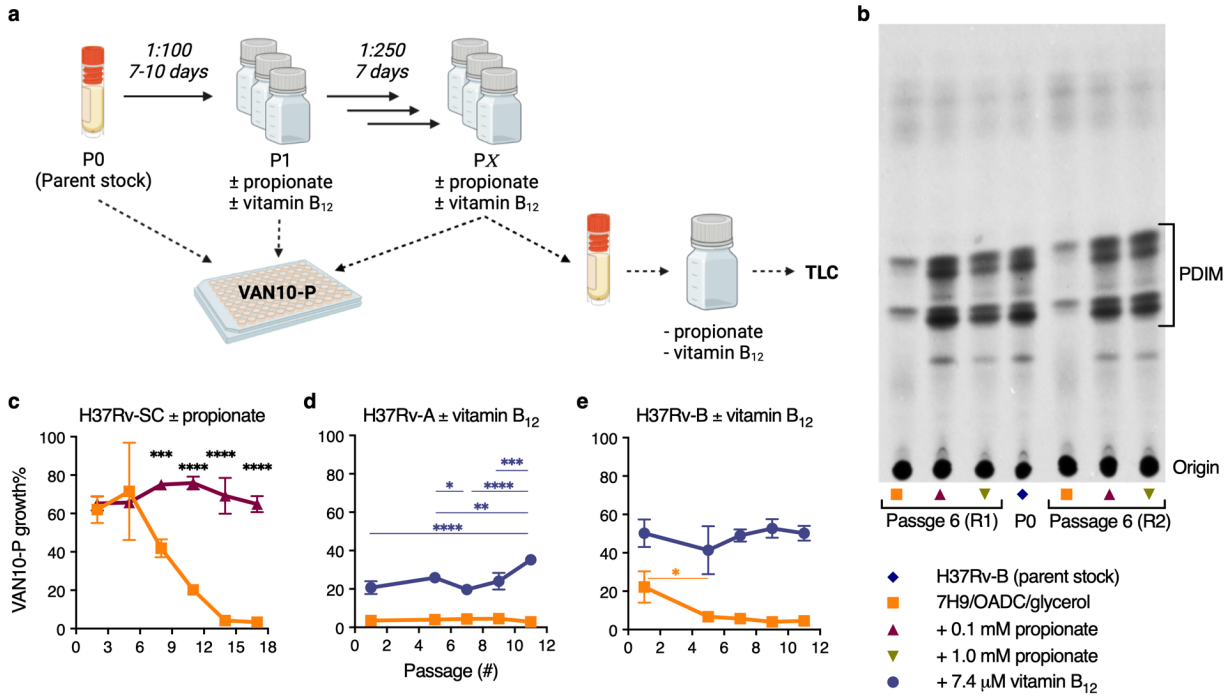

925

926 **Extended Data Fig. 8 | Propionate and vitamin B_{12} supplementation prevent PDIM loss in**
927 ***Mtb*. a**, Schematic overview of *in vitro* evolution experiments. Triplicate inkwells containing
928 standard 7H9/OADC/glycerol/tyloxapol or media supplemented with propionate or vitamin B_{12}
929 were inoculated with frozen *Mtb* culture stock (P0) and incubated for 7-10 days (P1). Cultures
930 were then diluted into fresh media every 7 days for serial passage (P2 to P*X*). Selected passages
931 were input into VAN10-P assays at the time of passage to assess PDIM production over the course
932 of the experiment. For TLC lipid analysis, frozen stocks were first outgrown in media without
933 propionate or vitamin B_{12} for a single passage to allow the strains to recover before ^{14}C-labelling.
934 Figure created with BioRender.com. **b**, TLC lipid analysis of H37Rv-B before and after six serial
935 passages in ± 0.1 or 1.0 mM propionate. This figure shows the full TLC plate from Fig. 4a with
936 results for both biological replicates analysed by TLC (R2 is shown in Fig. 4a). **c**, VAN10-P assays
937 for H37Rv-SC [PDIM(+) H37Rv wildtype] passaged in ± 0.1 mM propionate. **d**, H37Rv-A and **e**,
938 H37Rv-B passaged in ± 7.4 μM vitamin B_{12}. Mean ± SD for $n = 3$ biological replicates, each

939 assayed in triplicate. *$P < 0.05$, **$P < 0.01$, ***$P < 0.001$, ****$P < 0.0001$; two-way ANOVA
940 with Šidák's (**c**) or Tukey's (**d**,**e**) multiple comparison test. Significant differences between
941 conditions are indicated in (**c**) and between timepoints in (**d**,**e**).